

学位論文

Doctoral Thesis

Hearing impairment in *SMS1* deficient mice

(*SMS1* 欠損マウスにおける難聴)

呂 美紅

Lu Mei-Hong

熊本大学大学院医学教育部博士課程医学専攻知覚生理学

指導教員

宋 文杰 教授

熊本大学大学院医学教育部博士課程医学専攻知覚生理学

2012年9月

学 位 論 文

Doctoral Thesis

論文題名 : Hearing impairment in *SMS1* deficient mice
 (*SMS1* 欠損マウスにおける難聴)

著 者 名 : 呂 美紅
 Lu Mei-Hong

指導教員名 : 熊本大学大学院医学教育部博士課程医学専攻知覚生理学
 宋 文杰 教授

審査委員名 :	脳回路構造学担当教授	玉卷 伸章
	頭頸部感覚病態学担当教授	湯本 英二
	分子生理学担当教授	富澤 一仁
	形態構築学担当教授	福田 孝一

2012年9月

Contents

Abstract	III
List of reference articles	IV
Acknowledgement	V
Abbreviation list	VI
1 Introduction and Objectives	1
1.1 Introduction	1
1.1.1 Sphingolipids and sphingomyelin	1
1.1.2 Auditory system	2
1.1.3 Cochlear structures	6
1.1.4 Stria vascularis and endocochlear potential	8
1.1.5 Hearing impairment and related genes	10
1.2 Objectives	12
2 Materials and Methods	13
2.1 Genotyping	13
2.2 SMS1/2 gene expression in mouse inner ear	17
2.3 Behavioral tests	17
2.4 ABR measurements	20
2.5 Otoacoustic emission measurements	22
2.6 EP and K⁺ concentration measurements	25
2.7 Histochemistry	29
2.8 Western blotting	30
2.9 Hearing repair experiment	31
2.10 Data analyses	31
3 Results	33
3.1 SMS1 and SMS2 expression in mouse inner ear	33
3.2 Identification of SMS1- and SMS2- deficient mice and their littermates ..	34
3.3 Behavioral tests	35
3.4 ABR tests	37
3.5 Cochlear function in the KO mice	42
3.6 Cochlear histology	47
3.7 KCNQ1 expression in the marginal cells of SV	53
3.8 Pigmentation in the SV	56
3.9 Hearing repair	58

4	Discussion	60
4.1	Hearing loss in <i>SMSI</i> ^{-/-} mice, but not in <i>SMS2</i> ^{-/-} mice	60
4.2	Features of the hearing impairment in <i>SMSI</i> ^{-/-} mice	61
4.3	Mechanisms for hearing loss in <i>SMSI</i> ^{-/-} mice.....	62
5	Conclusion	67
	References	68

Abstract

Sphingomyelin (SM), a major species of sphingolipids, is a ubiquitous component of cell membranes and plays vital roles in signal transduction and cell growth and survival. However, its physiological functions have not been fully elucidated. Here we have examined the role of SM synthesis mediated by SM synthase (SMS) family members, SMS1 and SMS2, in auditory function. Hearing ability of SMS1 null mice, assessed with an association learning experiment and with auditory brainstem response, was impaired, especially at low frequency range; the impairment was accompanied by abnormalities of stria vascularis (SV), i.e., a decrease in the width of SV and a disorganization of marginal cells. Further, fluorescent immunostaining and western blotting revealed an altered expression pattern and reduced level of KCNQ1 channels in marginal cells. In addition, SMS1 knockout (KO) mice exhibited a significant decrease of endocochlear potential and distortion product otoacoustic emissions, suggesting the defects of cochlear functions. And observation of more macrophage invasion into SV at apical region than other regions may explain the low frequency hearing loss in these SMS1 KO mice. Mice lacking SMS2, however, showed no detectable hearing loss. Taken together, our results suggest hearing impairment in SMS1 deficient mice but not in SMS2 deficient mice. Defects in SV may at least in part account for the hearing impairment in SMS1 deficient mice.

List of reference articles

Companion article:

1. Mei-Hong Lu, Makoto Takemoto, Ken Watanabe, Huan Luo, Masataka Nishimura, Masato Yano, Hidekazu Tomimoto, Toshiro Okazaki, Yuichi Oike and Wen-Jie Song
Deficiency of sphingomyelin synthase-1 but not sphingomyelin synthase-2 causes hearing impairments in mice
J Physiol 2012, (in press).

Other articles:

1. Kazuya Yamagata, Takafuji Senoguchi, Mei-Hong Lu, Makoto Takemoto, Fazlul Karim, Chisa Go, Yoshifuji Sato, Mitustoki Hatta, Tatsuya Yoshizawa, Eiichi Araki, Junichi Miyazaki, Wen-Jie Song
Voltage-gated K⁺ channel KCNQ1 regulates insulin secretion in MIN6 beta-cell line
Biochem Biophys Res Comm, 407(3):620-5, 2011.
2. Masato Yano, Ken Watanabe, Tadashi Yamamoto, Kazutaka Ikeda, Takafumi Senokuchi, Mei-Hong Lu, Tsuyoshi Kadomatsu, Hiroto Tsukano, Masahito Ikawa, Masaru Okabe, Shohei Yamaoka, Toshiro Okazaki, Hisanori Umehara, Tomomi Gotoh, Wen-Jie Song, Koichi Node, Ryo Taguchi, Kazuya Yamagata, Yuichi Oike
Mitochondrial dysfunction and increased reactive oxygen species impair insulin secretion in sphingomyelin synthase 1 null mice
J Biol Chem, 286(5):3992-4002, 2011.

Acknowledgement

I would like to give my deepest gratitude to Prof. Wen-Jie Song and Dr. Kazuya Saitoh, my supervisors in my doctoral course, for their professional guidance, patience in supervisions, constant encouragement, and kind help in my daily life.

I would extend my sincere thanks to all members in our lab for their continuous encouragement and help in the past four years. I especially express my gratitude to Dr. Makoto Takemoto for his instructions to animal producing and techniques for histological experiments. I especially express my appreciation and thanks to Dr. Masataka Nishimura for the guidance of software design and data analysis for auditory brainstem response. And I would like to thank Dr. Hasegawa for her help in my daily life, and thank Huan Luo for her encouragement.

I gratefully acknowledge the help of Drs. Hiroshi Hibino and Soichiro Yamaguchi for advice on K^+ concentration measurements, Dr. Kazuya Yamagata for advice on western blotting, and the Gene Technology Center in Kumamoto University for use of their equipments.

I wish to thank professors who give us lectures in the Graduate School of Medical Sciences, Kumamoto University. I benefit greatly from their lectures.

I would like to give my gratitude to my friends for their support and encouragement during four-year study period in Kumamoto University, Japan.

Finally, I would like to take this opportunity to thank my family for their understanding and encouragement for long time.

Abbreviation list

ABR: auditory brainstem response

DAPI: 4, 6-diamidino-2-phenylindole

DPOAE: distorted product of otoacoustic emission

EP: endocochlear potential

GAPDH: glyceraldehyde-3-phosphate dehydrogenase

KO: knockout

NAC: N-acetylcysteine

PBS: phosphate buffered saline

ROS: reactive oxygen species

RT: room temperature

SM: sphingomyelin

SMS: sphingomyelin synthase

SPL: sound pressure level

SV: stria vascularis

1 Introduction and Objectives

1.1 Introduction

1.1.1 Sphingolipids and sphingomyelin

Sphingolipids are predominantly found in the plasma membrane, and to a lesser extent in intracellular membranes (van Meer & Hoetzl, 2010). They are not merely structural components of biological membranes, but also play vital roles, particularly in signal transduction (Hannun & Obeid, 2002; Merrill, 2002; Spiegel & Milstien, 2002; Lahiri & Futerman, 2007). Of the simple sphingolipids, ceramide, ceramide-1-phosphate, and sphingosine have been shown to be involved in a number of cellular events such as proliferation, differentiation, motility, growth, senescence, and apoptosis. In addition, accumulating evidence indicates that sphingolipids are involved in neural functions such as channel gating (Ramu et al. 2006; Xu et al. 2008), synaptic transmission (Darios et al. 2009), and learning and memory (Dunbar et al. 1993; Inokuchi et al. 1997). Recently, several studies have suggested a role for sphingolipids in hearing. For example, knockout (KO) mice that are genetically devoid of ganglioside GM3 synthase exhibit complete hearing loss (Yoshikawa et al. 2009). Similarly, deficiency of the sphingosine 1-phosphate S1P₂ receptor also causes profound hearing loss (MacLennan et al. 2006; Herr et al. 2007; Kono et al. 2007).

Sphingomyelin (SM), a major species of sphingolipids, is a ubiquitous component of cell membranes in organisms ranging from mammals to protozoa, and is by far the most abundant sphingolipid. It consists of a ceramide core, in which sphingosine bonded to a fatty acid via an amide linkage. In addition, it contains a polar head group, which can be either phosphocholine or phosphoethanolamine. The synthesis of SM from ceramide and phosphatidylcholine is mediated by SM synthase (SMS). Increasing evidence has indicated that SM synthesis is critical for cell survival and proliferation. In lymphoid cells, the activation of SMS restored cell growth ability of SMS deficient cells and prevented apoptosis (Yamaoka

et al. 2004). SMS overexpression or knockdown has been linked to mitogenic and pro-apoptotic pathway in mammalian cells (Ding et al. 2008; Riboni et al. 2001). Moreover, report has been provided that active SM synthase can also mediate signal transduction. NF- κ B signaling pathway was strictly controlled by ceramide level mediated by SM synthesis in WI38 human lung fibroblasts (Luberto et al. 2000). SMS is subcategorized into the family members SMS1 and SMS2 (Huitema et al. 2004; Yamaoka et al. 2004; Tafesse et al. 2006). While SMS1 is localized in the Golgi apparatus, SMS2 is found in the plasma membrane in both neuronal (Kidani et al. 2012) and non-neuronal cells (Huitema et al. 2004). The expression of both enzymes has been studied at the organ level, and is found in a variety of organs including the brain (Huitema et al. 2004; Yang et al. 2005). Recently, it has been shown that SMS1-deficiency impairs endocrine (Yano et al. 2011) and immune (Dong et al. 2012) functions, while SMS2-deficiency ameliorates high-fat diet-induced obesity (Li et al. 2011; Mitsutake et al. 2011), attenuates lipopolysaccharide-induced lung injury (Gowda et al. 2011), reduces atherosclerosis (Liu et al. 2009), and reduces the expression of drug transporters in the brain (Zhang et al. 2011).

SM is hydrolyzed into phosphocholine and ceramide by sphingomyelinase (Jung et al. 2000; Hannun & Obeid, 2002). A previous study reported that mutations of sphingomyelinase cause Niemann-Pick disease, which is associated with hearing loss (Konagaya et al. 1989). A recent study, however, reported normal auditory brainstem responses (ABR) in every subject in a sample of seven Niemann-Pick patients with sphingomyelinase-deficiency that were examined (Mihaylova et al. 2007). The relationship between SM metabolism and hearing thus requires further investigation.

1.1.2 Auditory system

Sound waves travelling through the ear canal will strike the tympanic membrane. This wave information travels middle ear via a series of delicate bones: the malleus, incus and stapes. These ossicles act as a lever and a teletype, converting the lower-pressure eardrum sound vibrations into higher-pressure

sound vibrations at another smaller membrane called the oval window (see Fig. 1-1). The sound information then converts to fluid waves in the cochlea. The fluid waves, in turn, cause the vibrations of the basilar membrane, on which sit the sensory hair cells which transforms mechanical waves to electric signals in neurons. Auditory signal was sent to brain through the auditory nerve projected from the hair cells. Before reaching the auditory cortex, auditory stimuli travel through the cochlear nucleus and superior olivary complex in the brainstem, the lateral lemniscal nuclei and inferior colliculus in the midbrain, and the medial geniculate body in the thalamus (see Fig. 1-2).

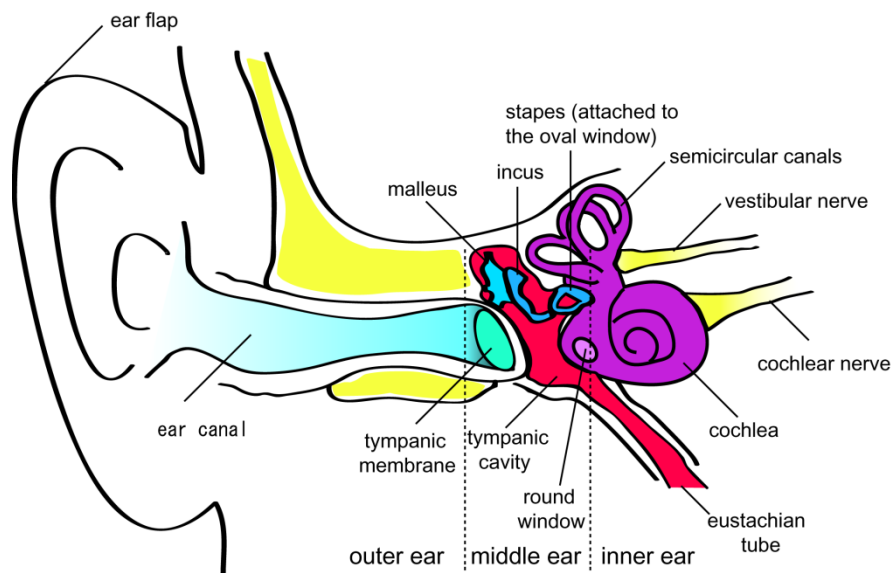


Fig. 1-1. Anatomy of human ear. The ear consists of three parts, outer ear, middle ear and inner ear (shown by two dashed lines). (Adapted from Chittka & Brockmann, 2005).

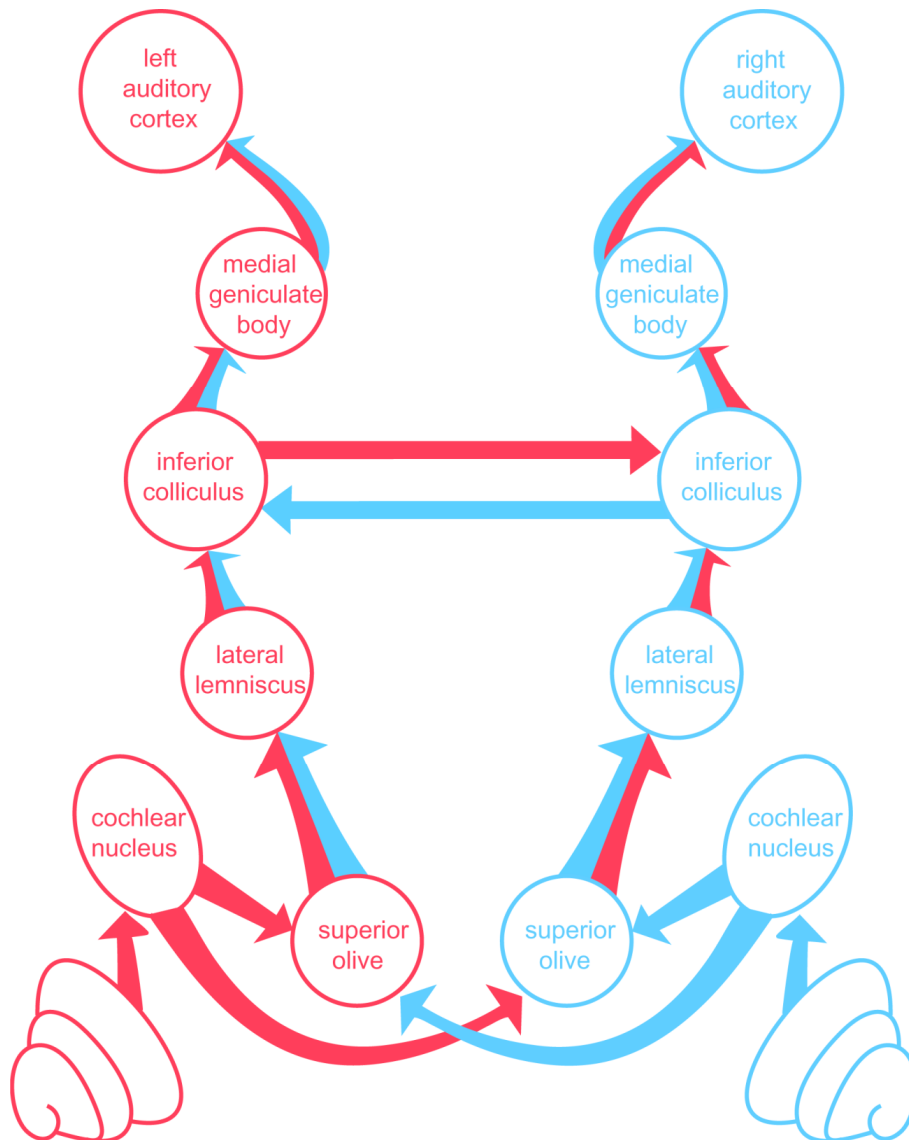


Fig. 1-2. Auditory pathway. The bilateral central auditory system, the main pathways and nuclei are shown for both cochleae. Bilateral representation from binaural stimulation occurs at the superior olive and in all regions above. (Adapted from Lindsay & Norman, 1972).

Auditory perception is not simply a matter of detecting a sound stimulus. The information content of sound is a function of frequency composition. Animals have an audible hearing frequency range, for example, humans can hear sounds approximately within the frequencies of 20 Hz and 20,000 Hz. The frequency ranges from other mammals are shown in Table 1-1 (Fay, 1988). The position of a sensory hair cell along the length of cochlea determines the sound frequency to which it is most sensitive. In other words, incoming sound waves lead to fluid motions that vibrate the basilar membrane at different position depending on sound frequency. The hair cells located at the base of the cochlea are maximally stimulated by high-frequency sounds; those occupying the apical position respond best to the low frequency sound. The place-frequency maps of cochlea have developed in many species such as cat (Lieberman, 1982), gerbil (Müller, 1996), and mouse (Müller et al. 2005). Actually there is tonotopicity in each nucleus and cortical regions. In the mammalian primary auditory field, the tonotopic organization is band-like along isofrequency axis, and neurons within the isofrequency band are laterally connected (Ehret, 1997; Wallace et al. 2000).

Animal	Frequency range
Human	20 -20,000 Hz
Dog	up to 40,000 Hz
Cat	100 -0,000 Hz
Rat	200 -70,000 Hz
Mouse	1000-91,000 Hz
Guinea pig	500 -50,5000 Hz
Bat	1,000 -100,000 Hz
Dolphin	up to 150,000 Hz

Table 1-1. Audible frequency range of mammals (Fay, 1988).

1.1.3 Cochlear structures

The mammals have a snail-like cochlea, coiled to 2 and 3/4 turns in human ear, and 2 and 1/4 turns in mice ear. The cochlear duct is divided into three compartments by two membranes, the basilar membrane and the Reissner's membrane. Between these two membranes is the scala media, also named endolymph, whose ionic composition is like that of intracellular fluids: high potassium, low sodium and with calcium ions held to micromolar concentration (Bosher & Warren, 1978; Anniko & Wróblewski 1986). Scala media contains the sensory hair cells and the organ of Corti, which sits on top of the basilar membrane. The tectorial membrane, situating on top of the organ of Corti, is an extracellular auxiliary structure contributing to hair cell excitation (Lukashkin et al. 2010). The uppermost compartment in Fig. 1-3, bottom panel, is the scala vestibuli, which has direct mechanical communication with the stimulus-induced displacement of the middle ear. The lower compartment, the scala tympani, ends at the base turn by the round window, which releases the mechanical pressure for the cochlea. Both the scala vestibuli and the scala tympani are filled with perilymph, similar to the extracellular fluids, high in sodium and low in potassium.

There are two distinct groups of hair cells in the mammalian cochlea: inner hair cells and outer hair cells. They differ by position, number, innervation patterns and functions. In the mammalian cochlea, there are normally four rows of hair cells, including three rows of outer hair cells and one row of inner hair cells. The inner hair cells are close to the central axis of the cochlear coil. Approximately 95% of afferent fibers are postsynaptic to inner hair cells. As many as 20 afferent fibers contact a single inner hair cell (Kiang et al. 1982; Brown, 1987). In contrast, outer hair cells have fewer afferent contacts. Instead they are postsynaptic targets of projections from the olivary complex in the brainstem. As for their functional difference, it is well established that inner hair cells convert the sound to the nerve signal, and that outer hair cells are acoustical pre-amplifiers.

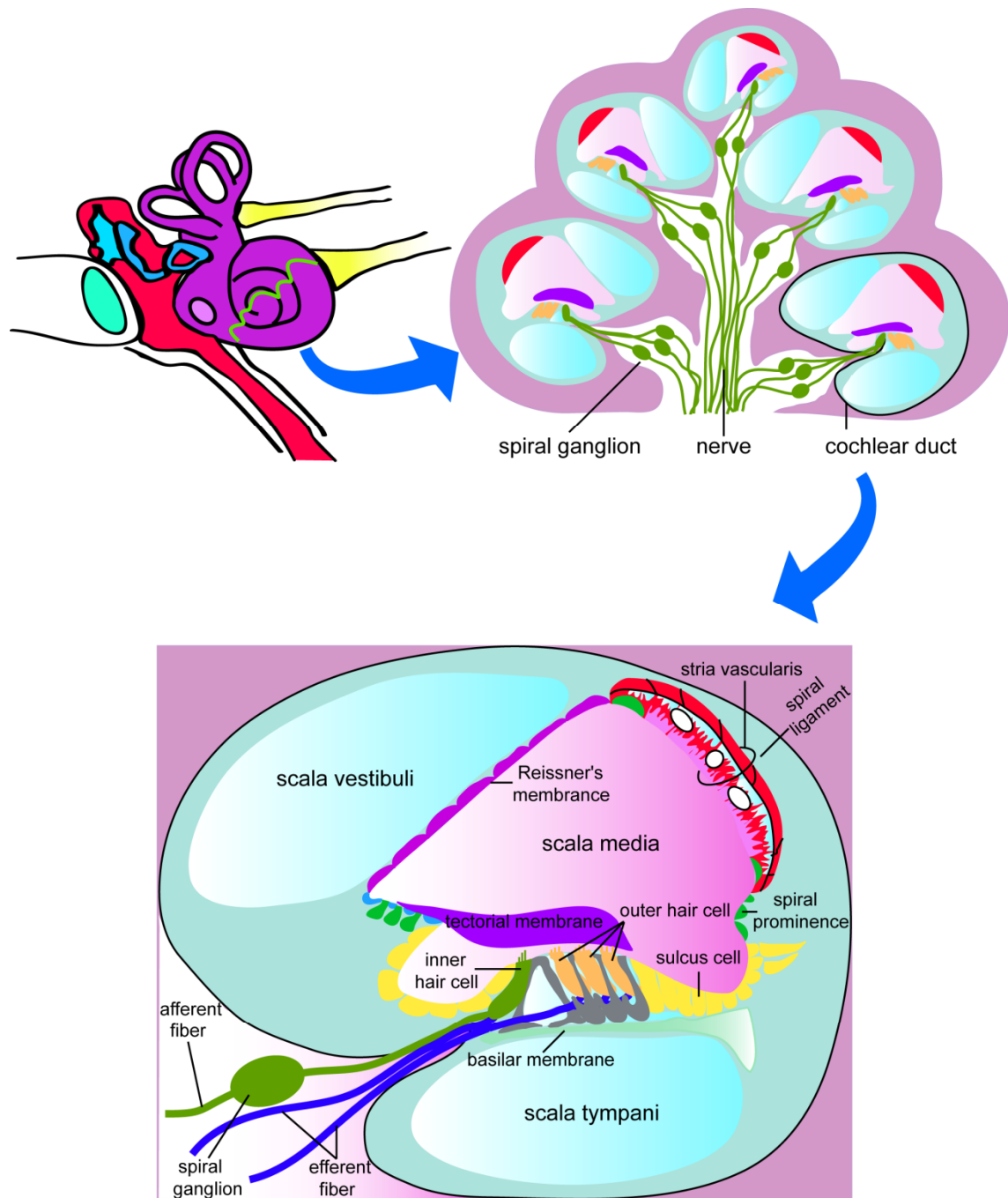


Fig. 1-3. Structure of cochlea. The upper left shows the snail-shell like cochlea. The upper right is the transverse section of cochlea. The below indicates the large view of cochlear duct. (Adapted from Zdebik et al. 2009).

1.1.4 Stria vascularis and endocochlear potential

The mammalian cochlea is a highly sensitive sensor of hearing; it can detect as small as 0.1 nm basilar-membrane vibrations induced by sound stimuli (Hudspeth, 2008). Endocochlear potential (EP) is one of important systems to achieve such exquisite sensitivity. It is the positive voltage of 80-100 mV seen in the endolymphatic space of the cochlea, only found in cochlear portion of the inner ear, and provides the main driving force for sensory transduction. Increasing reports have indicated that reduction or lack of EP in mouse models leads to serious hearing impairment even profound deafness (Gow et al. 2004; Kitajiri et al. 2004; Teubner et al. 2003; Wangemann et al, 2004; Rickheit et al. 2008).

The stria vascularis (SV) connecting with another compartment, the spiral ligament containing five types of fibrocytes, is considered as an epithelial tissue which is composed of marginal, intermediate, and basal cells (Fig. 1-4). The fibrocytes, basal, and intermediate cells are connected together through gap junctions, forming a barrier to separate the perilymph from the intrastria space, where there are numerous capillaries. Marginal cells constitute a monolayer of epithelia cells with their apical surfaces facing

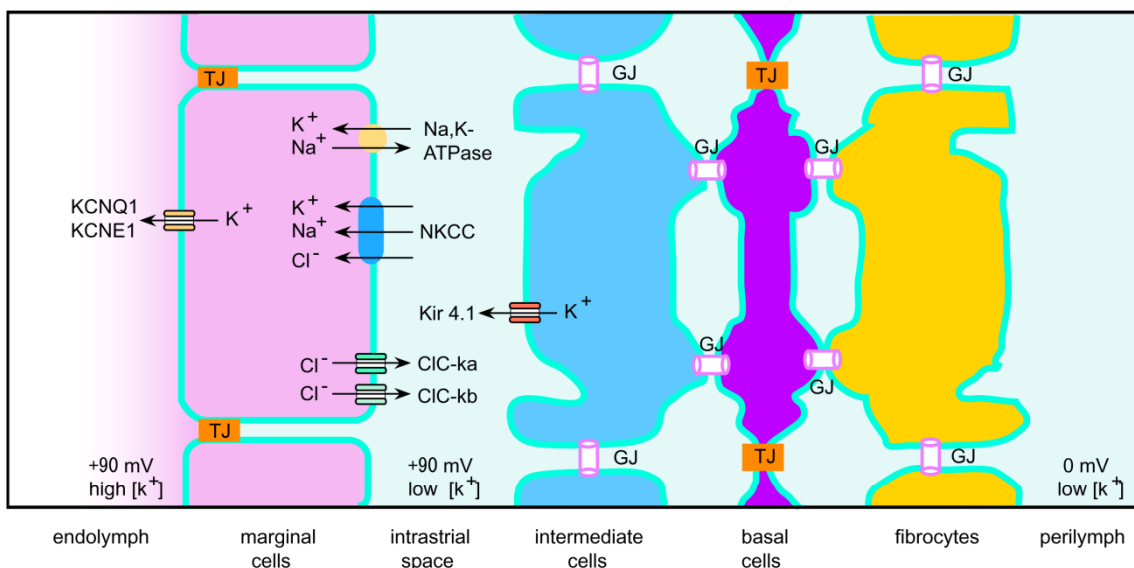


Fig. 1-4. SV structure and its transporters. GJ: gap junction; TJ: tight junction. (Adapted from Zdebik et al. 2009).

endolymph. These lined marginal cells directly secrete the potassium ion to the endolymph through the ion-transport apparatus to maintain the high potassium concentration in endolymph.

Concerns on the generation of EP have been taken into account since the first measurement of this potential. Tasaki and Spyropoulos (1959) have originally demonstrated that SV is essential for the formation of EP. In addition, ion transport apparatus have been demonstrated to be involved in the formation of EP. Na^+ , K^+ -ATPase, Na-K-2Cl cotransporter (NKCC), KCNQ1/KCNE1, and Kir4.1 are important molecules for K^+ circulation between endolymph and perilymph. The reduction or blockage of Na^+ , K^+ -ATPase and NKCC, which are expressed on the basal membrane of the marginal cells, caused dramatic EP decline (Konishi & Mendelsohn, 1970; Schulte & Schmiedt, 1992; Kusakari et al. 1978). Blockage of potassium channel by vascular perfusion of Ba^{2+} , sharply decreased the EP (Marcus, 1984; Hibino et al. 1997; Takeuchi et al. 2000). Moreover, mice lack of another potassium channel Kir4.1, which is expressed on the intermediate cells, exhibited abolishment of EP (marcus et al. 2002; Wangerman et al. 2004). Human Bartter syndrome IV characterized by congenital deafness, severe EP decline, renal salt and fluid loss is caused by mutations in BSND, which encodes barttin, a β -subunit of ClC-Ka and ClC-Kb chloride channels, suggesting that the EP is also dependent on the Cl⁻ channels (Rickheit et al. 2008). As for the mechanism for formation of the EP, the two-cell model, or five compartments model has been widely accepted (Takeuchi et al. 2000; Wangeman, 2002). Recently Nin et al (2008) and Hibino et al (2010) reported that three additional elements contribute to the EP other than the five compartments. The first one is the electrically separated barrier, the intrastria space. The second important factor is the K-diffusion potential at the apical surface of marginal cells. And the last point is another K-diffusion potential at the apical surface of the intermediate cells. More researches are still required to fully understand the mechanisms.

1.1.5 Hearing impairment and related genes

Hearing impairment is commonly caused by both environmental and genetic factors. Prolonged exposure of loud noise can lower the hearing sensitivity; even a sudden intense sound can lead to temporal or permanent hearing impairment (Davis et al. 1950; Kujawa & Liberman, 2009). Overdose of ototoxic drugs such as gentamicin has an adverse effect on hearing system and accounts for hearing loss (Yorgason et al. 2006). Genetic defects contributing to hearing impairments pose greater challenges. Research on this aspect has evolved rapidly over the past years. Animal models have provided a powerful tool for studying the underlying mechanisms of hearing loss that could not be achieved only by human studies. Mouse models have been proved to be an invaluable tool due to the striking similarities between mice and human in inner ear structure and functions (Probst & Camper, 1999; Friedman et al. 2007). The genes expressed in the ear must be considered first to be involved in hearing. Mutation of transporter gene *SCL26A4* (pendrin), which participates in maintaining the unique fluid homeostasis, leads to deafness (Coyle et al. 1998; Tsukamoto et al. 2003). A group of genes, *CLDN14*, *TRIC*, and *TJP2*, encode tight junction proteins and play a vital role in the formation of the mechanical barrier (Wilcox et al. 2001; Uyguner et al. 2003; Riazuddin et al. 2006). The myosin families of motor proteins, including MYO1A, MYO3A, MYO6, MYO7A, MYO15A, and MYH9, have a crucial role in hair bundle organization and function (Walsh et al. 2002). In addition, several extracellular matrix proteins such as tectorin, encoded by *TECTA*, have been associated with hearing (Verhoeven et al. 1998; Mustapha et al. 1999). In the present study, we found that deficient of *SMS1* accounted for hearing loss. It is not so surprising that numerous genes have been discovered to be involved in hearing impairment due to the complexity of hearing mechanisms. So far, more than one hundred of genes/loci have been linked to hearing loss (Fig. 1-5).

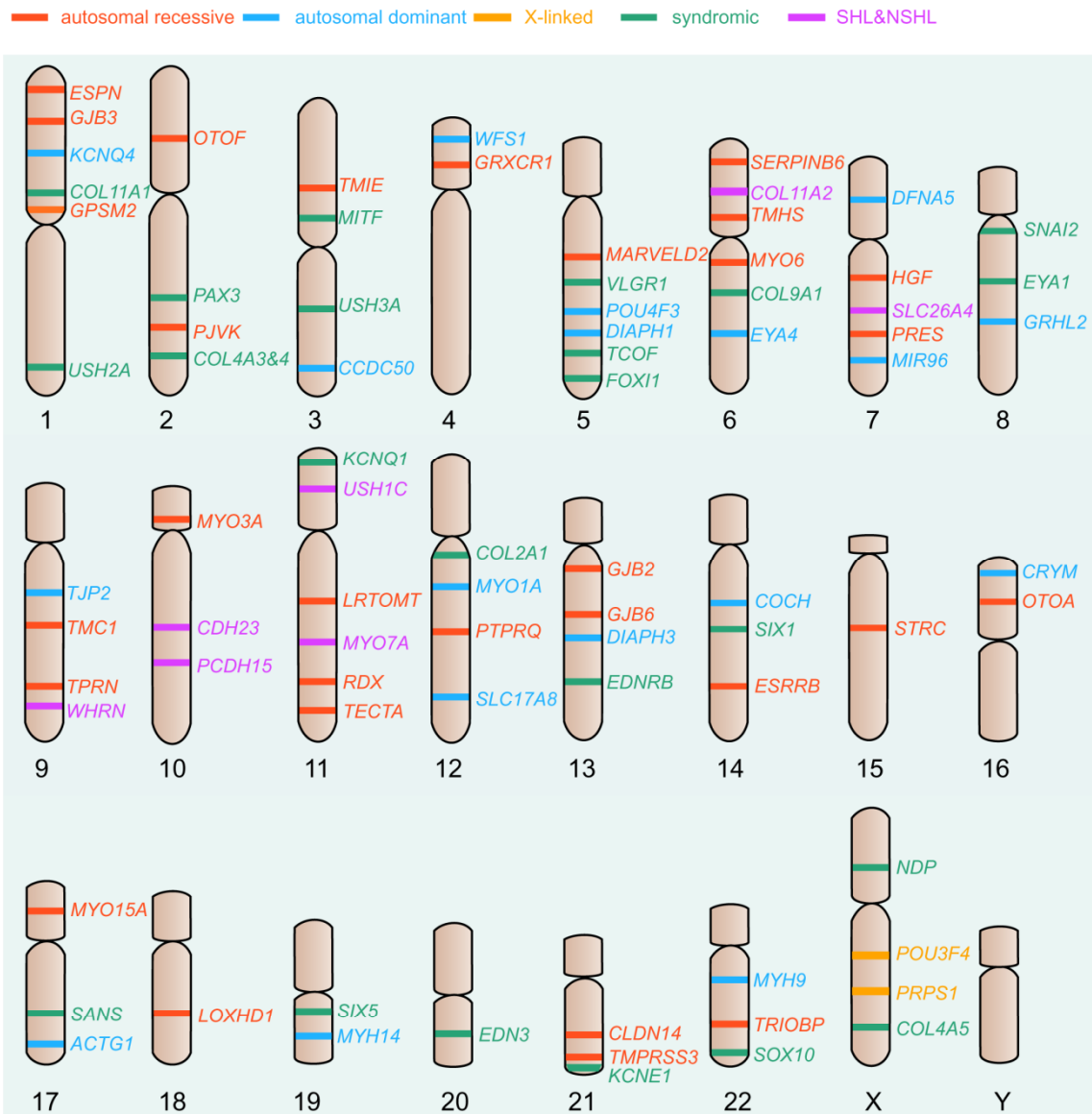


Fig. 1-5. The chromosomal location of genes with mutations causing hearing impairment in human. The genes are divided into five groups: nonsyndromic autosomal recessive (red), nonsyndromic autosomal dominant (blue), X-linked (yellow), syndromic (green), and genes that are associated with both syndromic and nonsyndromic hearing loss, SHL and NSHL for short (purple). All data were from the Hereditary Hearing Loss Homepage. (Adapted from Dror & Avraham, 2010)

1.2 Objectives

As mentioned above, most reports pertaining to SMS functions were based on molecular or cellular level. However, its physiological functions at organism level are still largely unknown and the functional differences between SMS1 and SMS2 were seldom reported, although one report indicated that SMS1 may represent a major SM synthesis activity in mouse lymphoid cells (Yamaoka et al. 2004) and another piece of evidence showed that co-expression of SMS1 and SMS2 are required to maintain SM homeostasis and growth in human Hela cells (Tafesse et al. 2007). Here, we addressed the relationship between SM metabolism and hearing by examining hearing ability in SMS1- and SMS2-deficient mice. Our results revealed that while *SMS1*^{-/-} mice showed progressive hearing loss in the low frequency range, the hearing abilities of *SMS2*^{-/-} mice were not different from their *SMS2*^{+/+} controls. In addition, we observed a decrease in the EP, atrophy of SV, and altered expressions of the KCNQ1 channel in the SV in the inner ear of *SMS1*^{-/-} mice. These findings may at least partially account for the hearing impairments in these animals. Moreover, the results also revealed a greater increase of macrophage invasion into SV at the apical region compared with the basal region of the cochlea in *SMS1*^{-/-} mice, possibly explaining the frequency-dependence of hearing loss in the animals.

2 Materials and Methods

2.1 Genotyping

All experiments were approved by Committee for Animal Experiments of Kumamoto University, and carried out in accordance with the Guidelines for Animal Experimentation of Kumamoto University. *SMS1* KO mice were generated and genotyped as described previously (Yano et al. 2011). Exon 2 of *SMS1* gene isolated from a mouse 129/Svj was replaced by neo cassette (see Fig. 2-1). *SMS1* KO mice used in this study were based on a 129/Svj-C57BL/6 mixed background by heterozygous mating to produce deficient mice and their littermate controls. For genotyping, tail tips were collected from mice at 3 weeks of age, and then were digested in lysis solution. The following “alkaline lysis method” was used for rapid preparation of mouse tail lysate suitable for amplification with KOD FX (TOYOBO).

- 1) Mark ears with a punch plier, cut tail tips (~3 mm) and then transfer to a 1.5 ml tube.
- 2) Add 90 μ l of 50 mM NaOH to the tube and vortex well to immerse the tissue in the solution.

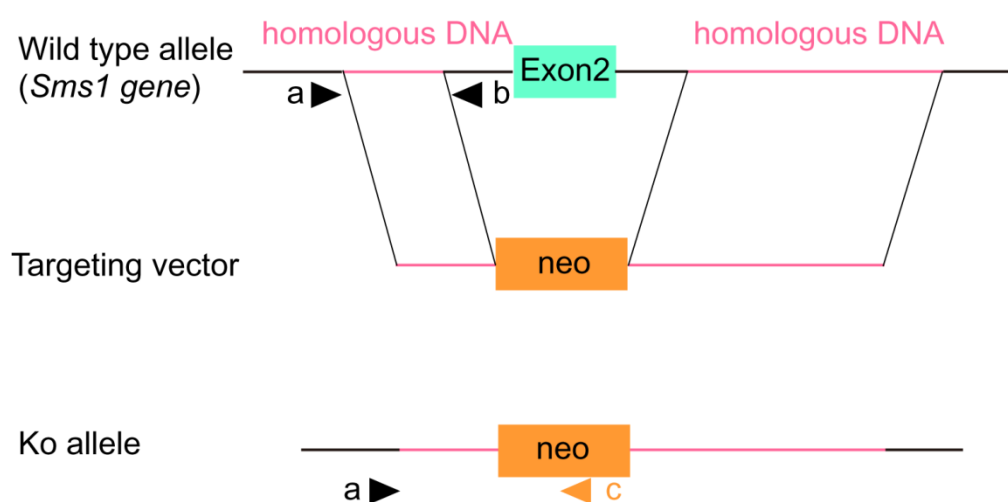


Fig. 2-1. Schematic representation of the targeting vector, the wild-type *Sms1* locus, and the mutant allele after homologous recombination. Exon is denoted by green box, which is replaced by neo cassette (orange box). Arrowheads are corresponding to the primer position to detect WT and KO alleles, respectively.

- 3) Incubate the tissue at 95 °C for approximately 15 min by using a heat block.
- 4) Add 10 µl of 1M Tris-HCl (pH 8.0) to the tube and vortex well.
- 5) Centrifuge at 12000 rpm for 5 min to sediment debris.
- 6) DNA samples can be stored at 4 °C or -30 °C until use.

Tail DNA was amplified with KOD kit (Toyobo) by using different pairs of primers. One forward primer GOR2SAp3 with the position of upstream of substitute fragment, and two reverse primers GOR2-R1 and PGKneoS, locating around exon 2 region deleted in KO mice and just inside the neo cassette, respectively, were used to distinguish WT, KO, and heterogeneous mice. The primer sequences are as follows:

a: GOR2SAp3, 5'-TTTGAGGAGAGAGGCCTTGAGTCTC-3'

b: GOR2-R1, 5'-AGGCAGCCACTTCCAGCAGCCAG-3'

c: PGKneoS, 5'-TCGCCTTCTATCGCCTTCTTGAC-3'

PCR reaction mixture was prepared as follows:

H ₂ O	0.6 µl
2x KOD Buffer	2.5 µl
dNTPs (2 mM each)	1.0 µl
GOR2-R4 (10 µM)	0.25 µl
GOR2-S1 (10 µM)	0.15 µl
Neo-F2 (10 µM)	0.15 µl
KOD polymerase (1 U/µl)	0.1 µl
Template	0.25 µl
Total volume	5 µl

Cycling parameters were set as follows:

Denature	95°C	2 min	
Cycle	98°C	10 s	15 cycles
	68°C	10 s	
Cycle	98°C	10 s	22 cycles
	58°C	30 s	
	68°C	30 s	
Polish	72°C	7 min	
Hold	4°C		

In this thesis, for all PCR product analysis, 1 μ l of 6 x agarose gel loading dye was added to 5 μ l of PCR reaction solution. After electrophoresis on a 1.5% agarose/TAE gel at 100 V for 40 min, the bands were stained with ethidium bromide and visualized by ultraviolet (Kodak). In *SMS1*^{+/+} mice, a 381-bp DNA fragment was obtained by using the primer set of GOR2SAp3 and GOR2-R1, while in *SMS1* KO mice, a 552-bp DNA fragment was amplified by the primer set of GOR2SAp3 and PGKneoS. Both above fragments were obtained in heterogeneous mice.

SMS2 deficient mice were generated by targeting exon 2 of *SMS2* gene and genotyped in a strategy similar to that used for *SMS1* KO (Mitsutake et al. 2011). Primers used to distinguish *SMS2* deficient mice from their littermate controls are as follows:

d: GOR1SAF1, 5'-CATTCTTGACTGTGTTCTGAGGATAC-3'

e: GOR1-R1, 5'-CCAAGTGCCTTCAAGTTTTGCTGTCTC-3'

f: NLSlacZ-R3, 5'-CAGGGTTTTCCCAGTCACGACGTTG-3'

Similar PCR reaction mixture was prepared as follows:

H ₂ O	0.55μl
2x KOD Buffer	2.5 μl
dNTPs (2 mM each)	1.0 μl
GOR1SAF1 (10 μM)	0.25 μl
GOR1-R1 (10 μM)	0.1 μl
NLSlacZ-R3 (10 μM)	0.25 μl
KOD polymerase (1 U/μl)	0.1 μl
Template	0.25 μl
Total volume	5 μl

Cycling parameters for *SMS2* gene amplification were set as follows:

Denature	94°C	2 min	
	98°C	10 s	
Cycle	60°C	30s	30 cycle
	68°C	30s	
Polish	72°C	7 min	
Hold	4°C		

In *SMS2*^{+/+} mice, a 430-bp DNA fragment was obtained by using the primer set of GOR1SAF1 and GOR1-R1, while in *SMS2*^{-/-} KO mice, a 540-bp DNA fragment was amplified by the primer set of GOR1SAF1 and NLSlacZ-R3. Both above fragments were obtained in heterogenous mice.

2.2 *SMS1/2* gene expression in mouse inner ear

Mice were killed by cervical dislocation and then were decapitated quickly. The head was placed on ice and the skin and the skull were removed. After removal of the brain, the inner ear at both sides was dissected by forceps, and then cochlear part was separated from the vestibule system and semicircular canal. Tissues inside the cochlea were collected carefully by making a hole at the bottom of the cochlea that is close to the basal turn of the cochlea. Inner ear tissue RNAs were pooled from 3 mice, while SV and organ of Corti RNAs were prepared from 6 animals. Total RNAs from wide type C57BL/6 mice were isolated with TRIzol reagent (Invitrogen) in a routine way. The quantification of total RNAs was evaluated by the absorption value at 260 nm wavelength (GeneQuant, Pharma Biotech). Synthesis of cDNA from approximately 1 µg of total RNA was performed with a RT SuperScript reagent kit (Invitrogen) according to manufacturer's instructions. The integrities and quantities of the cDNA were confirmed by amplifying β -actin, with forward primer of “5'-GTGGGCCCGCCCTAGGCACCAG-3'” and reverse primer of “5'-CTCTTTGATGTACGCACGATTTC-3'”. PCRs of *SMS1* variances including *SMS1 α 1*, α 2, β and γ , and *SMS2* gene were respectively carried out with KOD kit, using the corresponding primers and conditions described previously by Yang et al. (2005).

2.3 Behavioral tests

Three-month-old male mice (7 *SMS1*^{+/+}, 8 *SMS1*^{-/-}, 6 *SMS2*^{-/-}) were used for behavioral experiments. After 24 hr of water deprivation in their home cages, the animals were transferred to a custom-made chamber without a ceiling, to receive conditioning to form an association between a 4 kHz pure tone and the presentation of water (Fig. 2-2). The tone was delivered through a speaker placed 45 cm above the chamber floor, to suppress changes in the sound pressure level (SPL) at the ear of the animal due to changes in location and orientation of the animal. A camera was also set beside the speaker to monitor the behavior of the animal. A metal licking spout was fixed to one wall of the chamber, which supplied the

water reward and also worked as a licking sensor (Fig. 2-2 B). Food was available constantly. Each training trial lasted for 10 s and the inter-trial interval was 30 s. The training lasted four days, and 1440 trials were performed per day. On the first day, the first spontaneous licking of the spout was rewarded with ~50 μ l of water, and this initiated the training. In 715 of the 1440 daily trials, 4 kHz pure tone pulses (250 ms in duration with 10-ms rise/fall ramp, 500 ms inter-pulse interval) were presented from the speaker for 10 s (Fig. 2-2 A). These trials are referred to as the rewarded trials. In each rewarded trial, the SPL of the tone was randomly selected from levels ranging from 45 dB to 75 dB with 5 dB steps between the levels, and water reward was supplied only when the animal licked the spout during the 10-s tone presentation. A high rate of trials with a licking response to a tone thus indicates a learned association between the tone and the water reward. In the remaining 725 trials, neither a tone nor water reward was presented, regardless of whether the animal exhibited spontaneous licking; these trials are referred to as unrewarded trials. Rewarded trials and unrewarded trials were intermingled randomly to eliminate the predictability of behavior being rewarded. The rate of trials with licking was calculated for unrewarded trials and rewarded trials with tones at each SPL. The rate of licking in unrewarded trials was regarded as random behavior. In a pilot study using *SMS1^{+/+}* mice, the rate of rewarded trials with licking, averaged across all SPLs, and the rate of unrewarded trials with licking appeared to stabilize starting in the third day of training. We thus used the results from the fourth day of training for the comparisons between unrewarded and rewarded trials, across mice of different genotypes.

Sound generation and delivery were performed using Tucker-Davis Technologies (FL, USA) System III hardware and software, as we have reported previously (Nishimura et al. 2007). The SPL was calibrated with a sound level meter (type 2610 with a model 4191 microphone, Brüel & Kjær, Nærum, Denmark). Water reward was controlled with an electromagnetic valve. Licking was measured using custom-made hardware and software, and this software also controlled the Tucker-Davis Technologies System III and the electromagnetic valve. In all rewarded trials, the percentage of trials with licking at

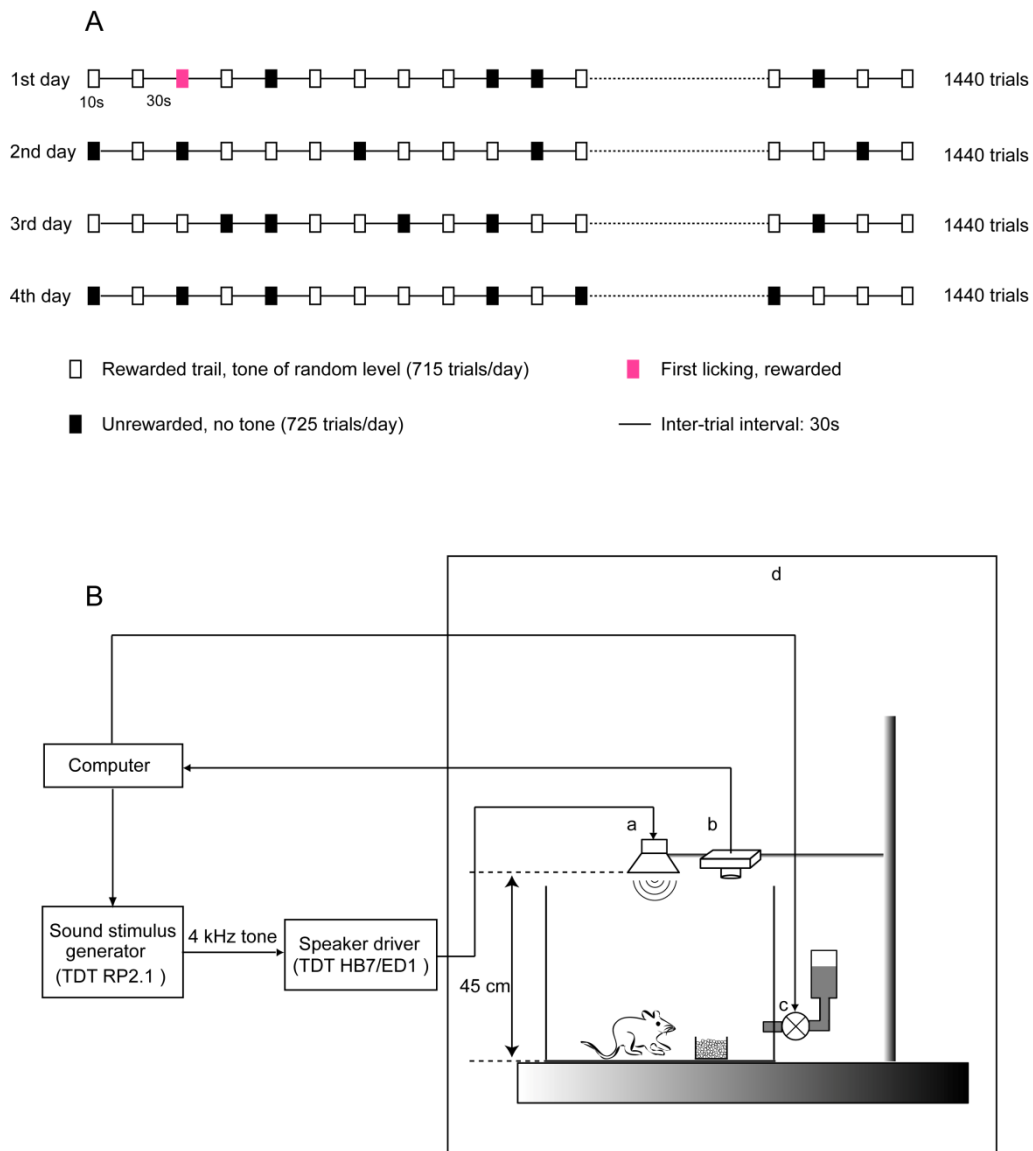


Fig. 2-2. Schematic illustration of behavioral test in mice. A, flow diagram of tone-reward association. Boxes indicated training rewarded (open), unrewarded (filled, black) and first spontaneous licking (filled, pink). The inter-trial interval was 30 s. The training lasted for four days. B, diagram of behavioral test system. Tests were performed in a sound-attenuated chamber (d). In a rewarded trial, sound was presented with random level by a speaker (a). Animal behavior was also monitored by a camera (b). The metal spout provided water, also worked as a sensor (c). Sound presentation, and water sensor were controlled by a computer.

different sound level was calculated by the following formula:

$$\text{Trials with licking at sound level of L (dB)} = \left(\frac{\text{Number of trials with licking at sound level of L}}{\text{Total number of trials at sound level of L}} \right) \times 100\%$$

2.4 ABR measurements

All mice were anesthetized with a mixture of ketamine (72 mg/kg weight) and xylazine (7.2 mg /kg). An adequate depth of anesthesia was verified by the absence of reflexes in response to toe pinches. Animals were then placed on a heating pad and the hairs over the head were cut to facilitate electrode attachment. ABRs to the acoustic stimuli were recorded as the potential difference between the left ear lobe and the vertex, using subcutaneous wire electrodes. Rectal temperature was measured with a probe inserted to a depth of about 2 cm (Fig. 2-3). The probe was lubricated by immersing in the oil prior to use to avoid injury to the animal. The body temperature was maintained at 38 ± 0.3 °C throughout recording using a thermostatically regulated heating pad. Click stimuli (one-cycle sine wave, 0.1 ms duration) and tone bursts (4-, 6-, 8-, 16-, 24-, 32-kHz; 1-ms rise/fall cosine ramp, 1-ms plateau) were generated digitally at a sampling rate of 97.7 kHz and delivered via a speaker positioned 10 cm from the ear. Sound stimuli were first applied at 20-80 dB SPLs with 10-dB steps between the levels to find the gross response threshold. The SPL was then finely adjusted from the gross threshold at 3-dB steps to determine the precise ABR threshold. The ABR threshold was defined as the lowest sound intensity at which the signal exceeded 3 times the SD of baseline noise (baseline: 10 ms recording before stimulus onset). The SPL was calibrated with a portable sound level meter (LA-5111, Ono Sokki, Kanagawa, Japan), which reported dB values close (± 2 dB) to those reported by the Brüel & Kjær calibration system mentioned above. For each stimulus condition, 3000 trials with an inter-trial interval of 0.1 s were conducted. The signal was amplified 100,000-fold, filtered (15 Hz-10 kHz), and averaged across the trials. In addition, the ABR interval from the first peak to the fifth peak in the ABR waveform in response to 60-dB sound

was measured to roughly evaluate the conduction time. All data acquisitions and analyses were conducted with custom-made software. Recordings were made in a sound-attenuating chamber (Fig. 2-3).

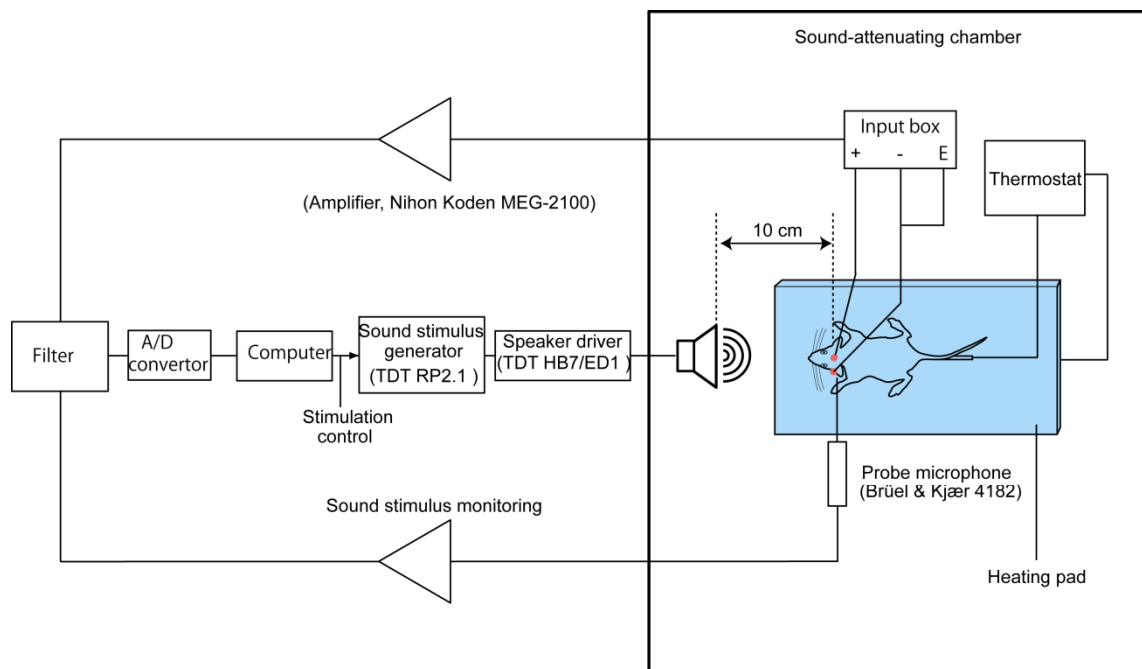


Fig. 2-3. ABR recording system. The rectal temperature of the animal was monitored and maintained by a thermostat. Sound was generated by TDT PR2.1 and its presentation was controlled by a computer.

2.5 Otoacoustic emission measurements

All mice were anesthetized as described above. One piece of head skin (2.5 cm x 1.5 cm) was removed to exposure the skull, on which three holes were drilled for screws to combine with the skull (Fig. 2-4 A and B). A mixture of liquid (monomer) and powder (polymer) of "REPAIRSIN" (GC Corporation, Tokyo) was applied to the mouse skull (Fig. 2-4 C). Before solidification, a thin and rectangular metal plate with one end having holes for fixing the animal head was stuck to that mixture. Pinnae of mice were cut to visualize the external canal and tympanic membrane and to verify the normal appearance of the membrane. A probe microphone/speaker system with two speaker ports (ER10B+, Etymotic Research, Inc.) was fitted tightly into the ear canal (Fig. 2-5 B). Two closed-field speakers (EC-1, Tucker-Davis Technologies, Inc.) were connected to the ER10B+ ports. Two primary tones (1 s duration with 20 ms rise/fall cosine ramp; $f_2/f_1=1.22$, f_2 varied at a one-fourth octave step from 4 kHz to 29 kHz) were generated as described above and routed separately to the two EC-1 speakers, at $SPL_1 = 75$ dB and $SPL_2 = 65$ dB. The SPL was calibrated in a 0.1 ml coupler (Polesskaya et al. 2010), using a Brüel & Kjær 1/4" pressure field microphone (model 4938), which has a flat frequency response from 4 Hz to 70 kHz (Fig. 2-5 A). The calibration was conducted for primary tones and all distortion products of otoacoustic emission (DPOAE) components. As shown in the Fig. 2-5 C, the DPOAE response from the ER10B+ microphone was amplified by 20 dB and digitized at 150 kHz using an A/D convertor (PCI-MIO-16E-1, National Instruments, Inc.). All data acquisitions and analyses were performed using custom software written in Matlab (MathWorks, Inc.). The recordings were repeated 10 times at an interval of 20 s and averaged in the time domain. The noise level was estimated by averaging three adjacent frequency bins that were above and below the DPOAE frequency.

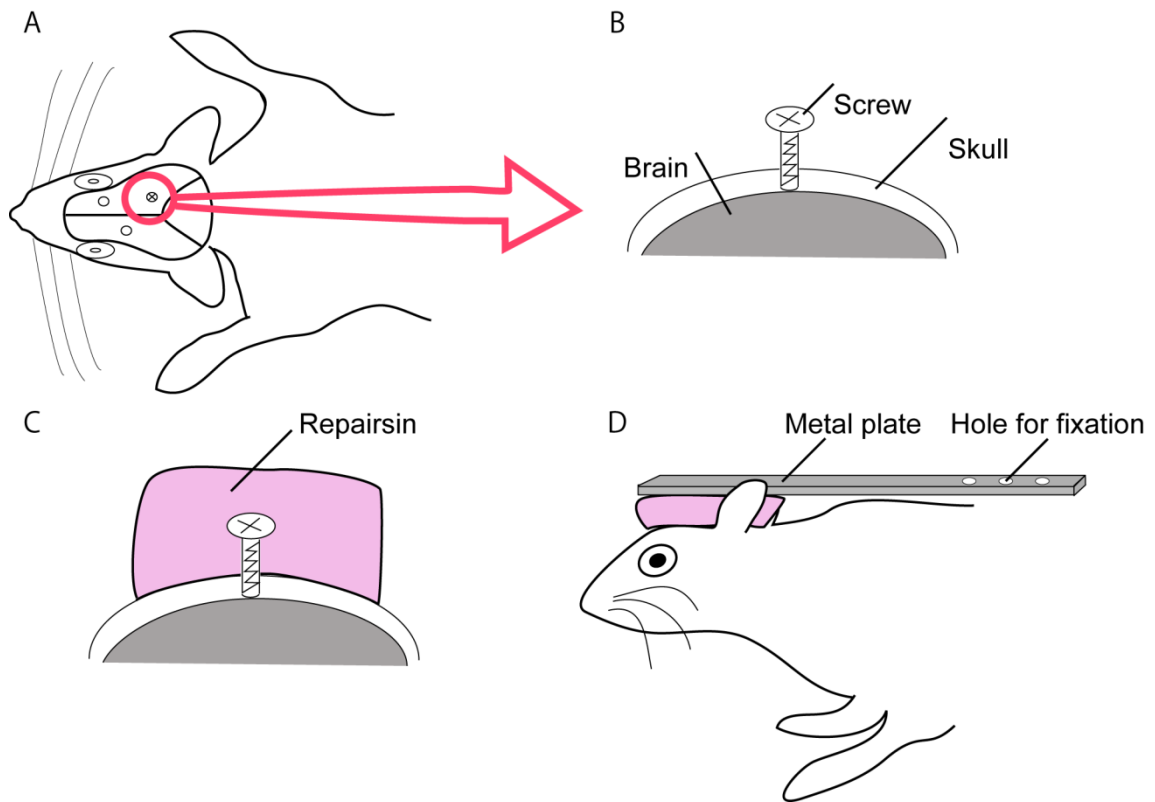


Fig. 2-4. Schematic illustration of mouse head fixation for DPOAE recording. A, the mouse skin over the head was removed to expose the skull. Mouse skull was screwed by making three small holes on the skull. B, the circled area in A. C, repairsin was used to attach the screw. D, a metal plate on the skull. The screw helped to strengthen the attachment. The head of the animal can be fixed well through the hole in the metal plate.

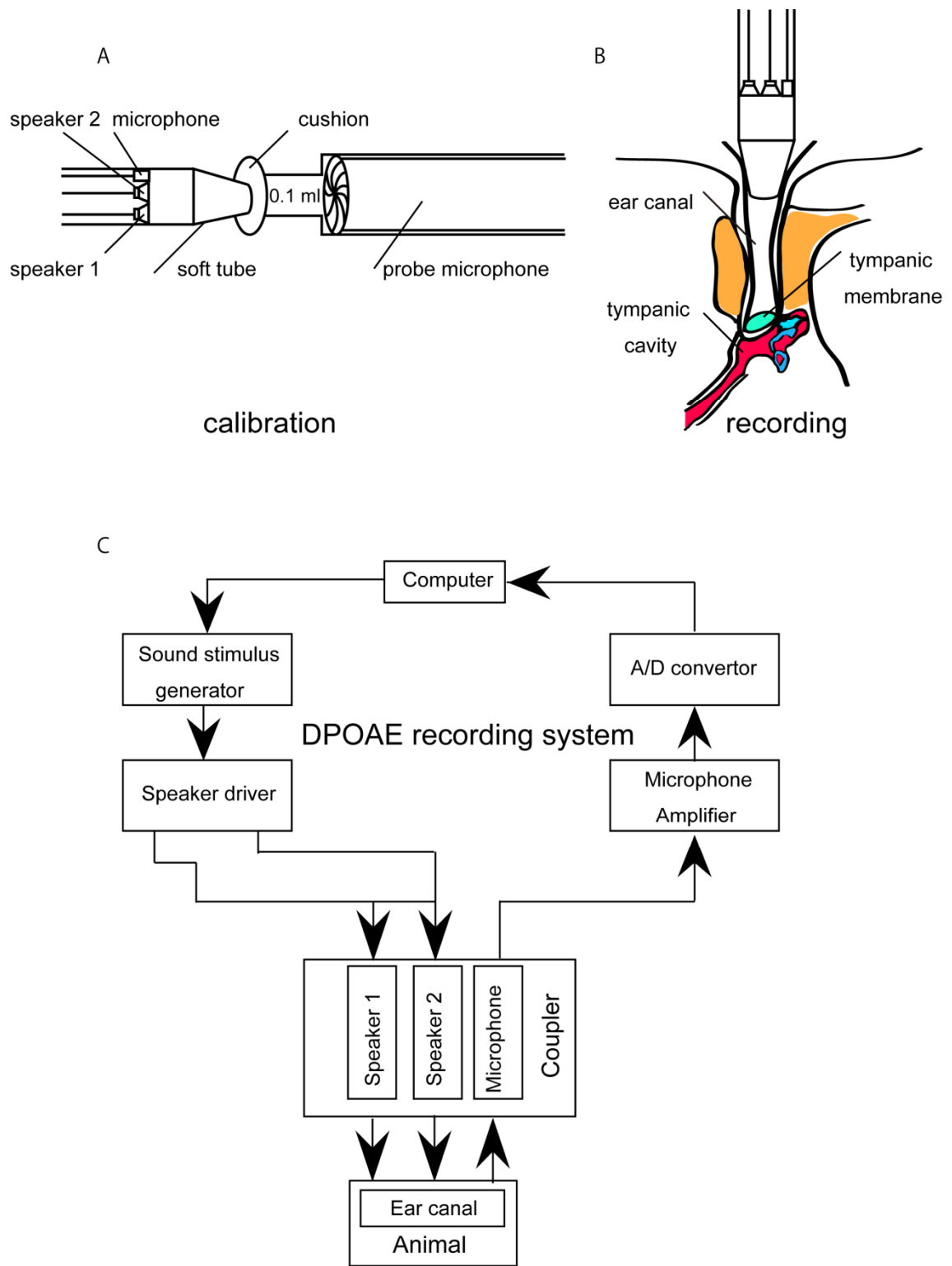


Figure 2-5. DPOAE measurement in mouse. A, schematic illustration of sound calibration from two speakers. B the connection between the ear canal and the probe comprising of the speakers and microphone. C the DPOAE recording system.

2.6 EP and K⁺ concentration measurements

EP and K⁺ concentrations were measured simultaneously using a double-barrel electrode in mice anesthetized as described above, following methods reported previously (Nin et al. 2008). After trimming one barrel by about 1cm (Fig. 2-6 C) using a supersonic knife (USW-335Ti, Honda Electronics), double-barrel electrodes were pulled from borosilicate glass capillary (inner diameter: 0.86mm; outer diameter: 1.5 mm; Sutter) with tip diameter about 1 μ m (P-87, Sutter). A chamber comprising of a 15-cm-diameter glass dish and a drilled metal plate (Fig. 2-6 A, B and D), which was sealed on top of the dish with Sylgard (Dow Corning), was dried for 0.5 hr at 200 °C in an oven prior to each experiment. The microelectrodes were vertically set on the chamber (Fig. 2-6 D), with the longer part of the untrimmed barrel inserted to a hole. And the chamber with electrodes was dried for another 0.5 hr at 200 °C in an oven. After injection of 500 μ l dimethyldichlorosilane (5% in toluene) to the chamber using a 1 ml syringe, the microelectrodes were baked for 2 hr at 200 °C. The silanized barrel was filled with a K⁺ exchanger solution (IE190, WPI) in the tip with a length about 500 μ m without bubbles by checking under a microscope, and back filled with a 150 mM KCl solution, to measure the K⁺ concentration. The other barrel was filled with a 150 mM NaCl solution to measure the EP. Each barrel was connected to a separate channel of a high-impedance dual channel electrometer (FD223a, WPI). The amplifier was kept in “STANDBY” mode until the probe is connected to the measurement site, and then the select toggle may be changed to “OPERATE” mode during recording. A reference AgCl electrode was placed in the neck muscle. Signals from the electrometer were amplified and digitized at 100 Hz using an A/D convertor (NI9205, National Instruments, Inc.). All data acquisitions and analyses were performed using custom software written in Matlab (MathWorks, Inc.). For recording, the animal was placed on a heating pad, and its head was fixed as described in DPOAE recordings part (see Fig. 2-4). By a lateral approach, the pinna, the muscle and the ear drum were removed by forceps and scissors along the ear canal to expose the cochlea under a stereomicroscope (Olympus). To visualize the cochlea clearly, part of the

tympanic bulla was also removed by a rongeur. A small hole was carefully made in the middle turn of the cochlea to expose the spiral ligament, using a fine drill (Fig. 2-7 A). The electrode was advanced through the spiral ligament by means of a micromanipulator (PC-5N, NARISHIGE), and a sudden increase of the potential signaled the entrance of the microelectrode tip into the endolymph. Recordings were used for analysis only when the EP was stable for > 1 min. Before and immediately after each experiment, the ion exchanger-filled microelectrode was calibrated using a series of KCl solutions that ranged in concentration from 5 mM to 160 mM with the background of NaCl solution (see Table 2-1). All solutions were maintained at 38 °C by a thermostatic waterbath. Noise was shielded using a metal covering. In addition, a salt bridge and a reference electrode (DRIREF-2SH, WPI) were used to lower the noise and keep the signal stable during experiment (see Fig. 2-7 B). The calibration voltage at 5 mM KCl was set a constant value, for example 40 mV, and values were obtained at other concentrations in the order from 25 mM to 160 mM KCl solution. The results of the calibration were fitted with the Nicolski equation in the following form, with KaleidaGraph (version 4.0): $V = V_0 + S \cdot \log (a \cdot [K^+] + A \cdot a \cdot [Na^+])$, where $V = K^+$ potential, $V_0 =$ offset, $S =$ slope, $a =$ activity coefficient, and $A =$ ion selectivity. Only electrodes having a slope greater than 55 mV per 10 fold increase in ionic strength were used for recording. Recordings were used for analysis only when the difference in the values of the slopes obtained from the calibrations before and after the recording was less than 2%. The endolymph K^+ concentration was determined from the calibration curve obtained after each recording, using the voltage difference between the potential from the ion exchanger-filled barrel and the EP. When the double-barrel microelectrode touched the spiral ligament, we zeroed the potential from both barrels since potassium concentration in external solution of cochlea is close to 5 mM. Thus in every experiment, finally adequate amount of standard solution of 5 mM KCl with 155 NaCl was applied to the tympanic cavity and the potential difference between the two barrels was measured in this solution to calibrate this value.

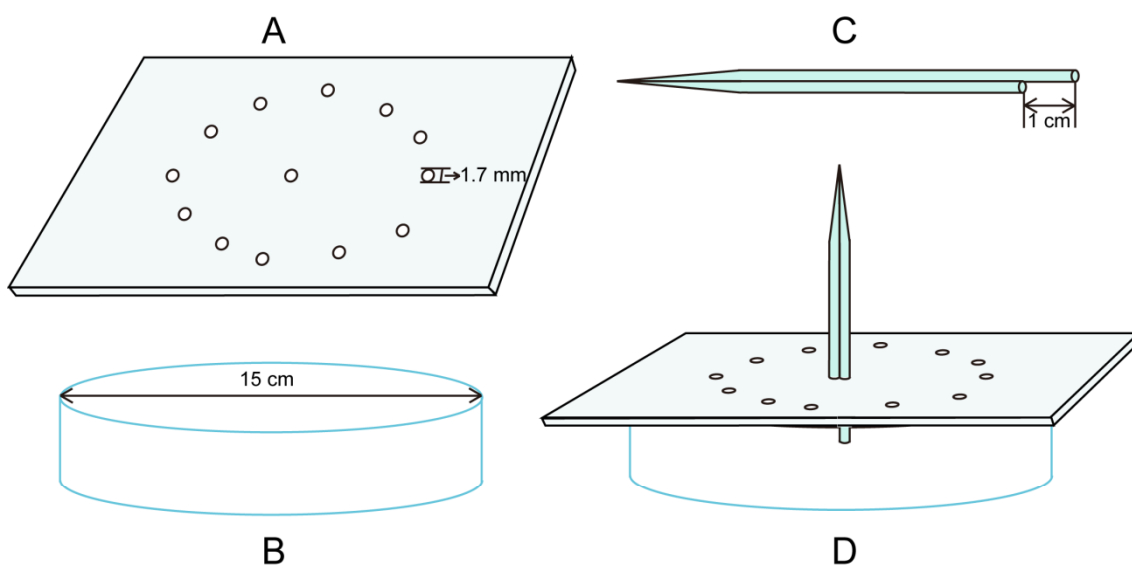


Fig. 2-6. Fabrication of microelectrodes. A heatproof metal plate (*A*), with drilled holes (with the diameter of 1.7 mm), was sealed to a glass Petri dish (*B*) using Sylgard to make a chamber (*D*). As shown in *C*, one barrel of double-barrel microelectrode was trimmed for about 1 cm at the end, and the longer barrel was situated on the chamber vertically for silanizing the tip.

NO.	KCl (mM)	NaCl (mM)	Total (mM)
1	5	155	160
2	25	135	160
3	50	110	160
4	80	80	160
5	120	40	160
6	160	0	160

Table 2-1. Standard KCl solutions for calibration

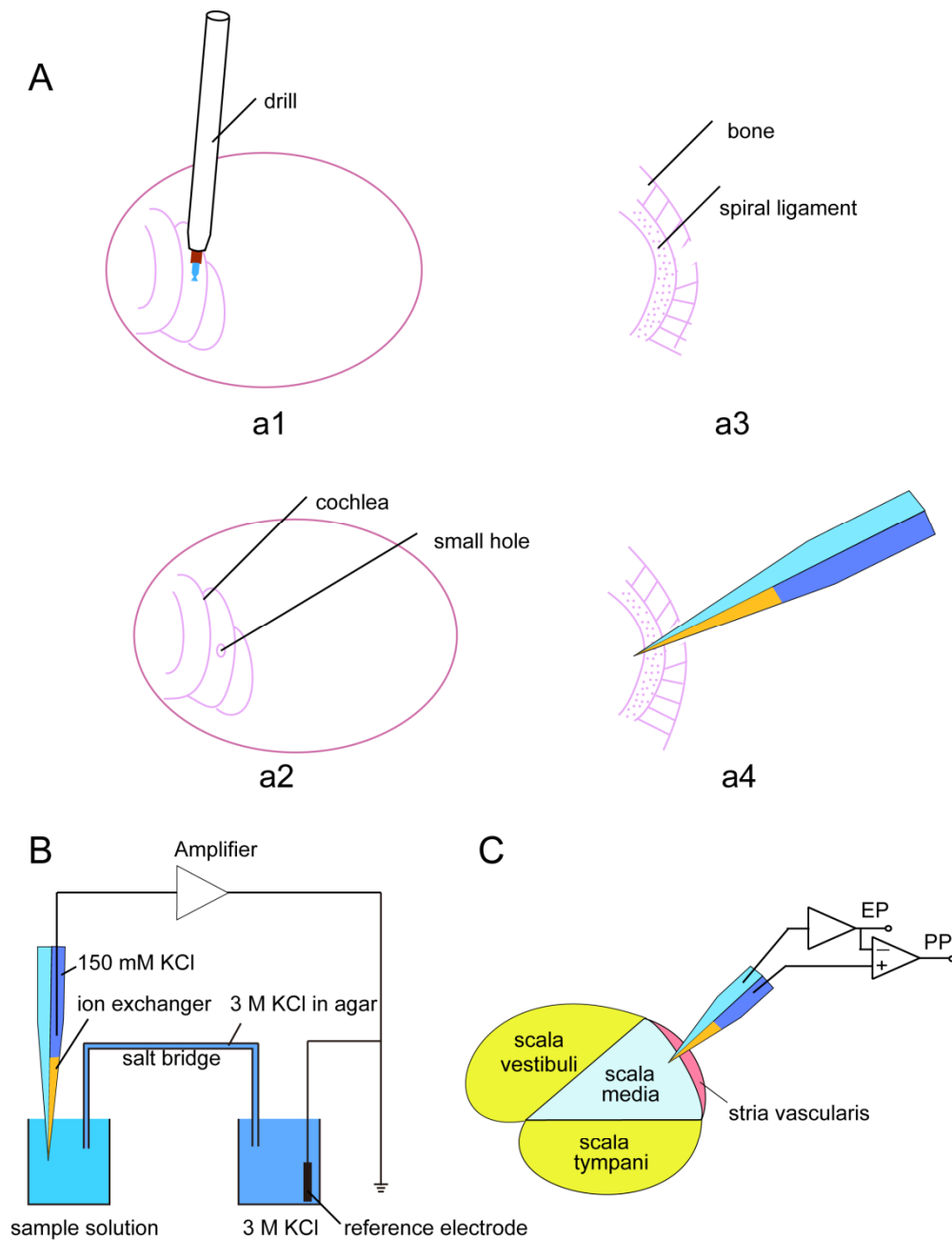


Fig. 2-7. Schematic illustration of calibration of ion selective microelectrodes, and EP and endocochlear potassium concentration measurements. *A*, The cochlea was exposed by a lateral approach. A small hole was made on the middle turn of cochlea by a fine drill (*a1*, *a2*). Bone over the spiral ligament was thinned (*a3*), and the microelectrode was inserted to the endolymph through the hole (*a4*). *B*, a schematic diagram illustrating the method for calibration. *C*, simultaneous recording of the EPs and K^+ potentials (PPs).

2.7 Histochemistry

Animals were transcardially perfused with 4% paraformaldehyde in 0.1 M phosphate buffer under deep anesthesia (ketamine 120 mg/kg and xylazine 10 mg /kg). The inner ear at both sides was then harvested as described above and fixed in 4% paraformaldehyde for additional 1-2 days, before decalcification with 10% ethylenediamine tetraacetic acid for 2 days at room temperature (RT) or 3 days at 4 °C. In each animal, one cochlea was sectioned, whereas the other cochlea was used for flat-mount tissue preparations. For sectioning, the decalcified cochlea was cryoprotected in a series of sucrose in phosphate buffered saline (PBS) solutions. A cubic plastic chamber full of TOC was used to fix the cochlea with the cochlear axis parallel with the horizontal plane, and rapidly frozen on a flat block of dry ice. The chamber containing the cochlea was transfer to the cryostat precooled for 0.5 hr. After removal of the plastic chamber, the tissue-containing TOC block was fixed with its bottom surface parallel with the blade. In doing so, transverse sections can be obtained. The cochlea was sectioned at a 10- or 6- μ m thickness. For flat-mount preparations, the cochlea was dissected into apical, middle, and basal turns. Then, the basilar membrane including the organ of Corti and the cochlear lateral wall tissues including the SV were separated. The tissue was then cut into several pieces to allow them to be flattened on a glass slide.

F-actin staining was performed by incubating pieces of decalcified cochlear tissues in rhodamine-conjugated phalloidin (Invitrogen R415, 1:200) in PBS with 0.1% Triton X-100 for 30 min at RT. After several times washing, the tissue pieces were mounted on glass slides with the hair cells uppermost for basilar membrane staining or marginal cells uppermost for lateral wall staining. The hair cells or the marginal cells were visualized under a microscope.

To visualize the vasculature in SV, the SV fraction was dissected out and fixed in 4% paraformaldehyde for 30 min on ice. The tissue was treated in blocking buffer (2% bovine serum albumin in PBS with 0.1% Triton X-100) for 1.5 hr at RT. And then the tissue was stained overnight at 4 °C with Alexa Fluor 594-conjugated isolectin GS-IB4 (4 μ g/ml, Molecular probes) in blocking buffer containing 1

mM CaCl₂ and 1mM MgCl₂. After several times washing in PBS, the tissue was mounted on a glass slide with the marginal cells uppermost.

For KCNQ1 immunohistochemistry, cochlear sections were blocked with PBS containing 5% normal donkey serum and 0.1% Triton X-100 for 1 hr at RT. The sections were then incubated with a goat anti-KCNQ1 polyclonal antibody (Santa Cruz sc-10646, 1:200) overnight at 4 °C, followed by reaction with an Alexa Fluor 488-conjugated donkey anti-goat IgG (Invitrogen A11055, 1:500) for 1-2 hr at RT. All sections were counterstained with 4, 6-diamidino-2-phenylindole (DAPI).

2.8 Western blotting

Three-month-old *SMS1*^{+/+} and *SMS1*^{-/-} mice (10 of each genotype) were decapitated under deep anesthesia as described above and the cochlea was harvested. SV fractions from each genotype were dissected in cold PBS by fine forceps under a microscope, and collected to a 1.5 ml tube. The tissues were then lysed with a sample buffer (50 mM Tris-HCl, pH 6.8, 10% glycerol, 2% SDS, 0.1% bromophenol blue, and 6% 2-mercaptoethanol) overnight at 4 °C. Western blot analysis followed those described before (Yamagata et al. 2011). Samples were not subjected to heat treatment prior to western blot analysis to avoid degradation. Proteins were resolved at 20 mA/gel for 50 min by SDS polyacrylamide gel electrophoresis (12 well mini-gels, ATTO, Tokyo), and then transferred onto a polyvinylidene fluoride membrane at 150 mA/gel for 60 min in a semi-dry blotter (ATTO) with transferring buffer (25 mM Tris-HCL pH 8.3, 192 mM glycine, and 20% methanol). The membrane was blocked overnight at 4 °C in 5% skim milk dissolved in Tween-TBS (20 mM Tris-HCL pH7.6, 150 mM NaCl, and 0.1% Tween 20), and was incubated with anti-KCNQ1 antibody (Santa Cruz ,1:300, sc-10646) for 1.5 hr at RT in Tween-TBS containing 5% skim milk. Glyceraldehyde-3-phosphate dehydrogenase (GAPDH) was also analyzed as a control protein using an antibody from Sigma (G9545, 1:10,000). Proteins were visualized using ECL western blotting detection reagents (GE Healthcare) and images were obtained and analyzed

with a LAS 4000 imaging system (Fuji Film, Tokyo, Japan).

2.9 Hearing repair experiment

After weaned at three weeks of age, both *SMSI*^{+/+} and *SMSI*^{-/-} mice were separated from their mothers. They were kept in new cages and fed with water containing 40 mM N-acetylcysteine (NAC). The water bottle was covered with the foil to avoid light exposure. Food was available all the time. When the animal were 3 months old, the hearing ability was tested by ABR using both click stimulus and tones at different frequencies.

2.10 Data analyses

To quantify the apical membrane area size of the marginal cells, phalloidin-stained compartment boundaries were determined using NIH Image J software and manually verified. The area sizes were then measured using the software. For evaluating pigmentations in the SV, brightfield images of flat-mount SV tissues were acquired, converted into 8-bit images, and binarized after subtracting the background noise, again using Image J software. The percentage of total area of binarized signals, i.e., the pigmented area, to the area of SV was calculated and compared between *SMSI*^{-/-} mice and their *SMSI*^{+/+} littermates, at the apical and basal levels of the cochlea. For evaluating atrophy of the SV, the SV width (width along the base-to-apex direction) was measured as the distance between the two points of SV, where its thickness decreased to half of the maximum, along the SV surface; the ratio of the SV width to the width of the lateral wall in the scala media was then calculated. The width of the lateral wall was measured as the distance between its two ends, defined by the Reissner's membrane and the basilar membrane, respectively, along the lateral wall surface in the scala media. KCNQ1 expression at the apical surface of SV was evaluated by the ratio of KCNQ1-positive length to the width of SV.

All data are described either as mean \pm standard error of the mean (SEM) or as mean \pm SD (see Figure

legends). Student's t-tests were used to test for group differences. Differences were considered statistically significant if $p < 0.05$.

3 Results

3.1 *SMS1* and *SMS2* expression in mouse inner ear

As reported previously, alternative splicing of *SMS1* gene gives rise to four different transcripts, *SMS1 α 1*, *SMS1 α 2*, *SMS1 β* and *SMS1 γ* . However, three different proteins named SMS1 α , SMS1 β and SMS1 γ were translated due to the same protein, SMS1 α , coded by *SMS1 α 1* and *SMS1 α 2* genes. It is unclear whether *SMS2* gene has its variances. Tissue distribution of the *SMS1* transcripts and *SMS2* in mice has been investigated by Yang et al. (2005). They have reported that *SMS1 α 1*, *SMS1 α 2* and *SMS2* transcripts were widely expressed. The *SMS1 β* transcript showed a narrow distribution while the expression of *SMS1 γ* was detected only in the testis and heart of mouse. Thus they concluded that the regulation and function of different transcripts and proteins are likely to be tissue specific. Although many kinds of tissues, such as heart, brain, lung, liver and kidney have been analyzed, the expressions of these genes in mouse inner ears were never examined. In order to confirm this, RT-PCR analysis was performed using total RNA from mouse inner ear. Strong expressions of all *SMS1* transcripts except for *SMS1 γ* were detected. Similar to other tissues, inner ear tissue showed weak expression or no expression of *SMS1 γ* (Fig. 3-1 A). The organ of Corti and the SV are important structures for proper hearing. We next investigated the relative expression of these genes excluding *SMS1 γ* in these tissues based on semi-quantitative RT-PCR using *β -actin* as a control gene. All gene expressions showed a similar level between the organ of Corti and the SV except that *SMS2* exhibited a higher level in the organ of Corti (Fig. 3-1 B).

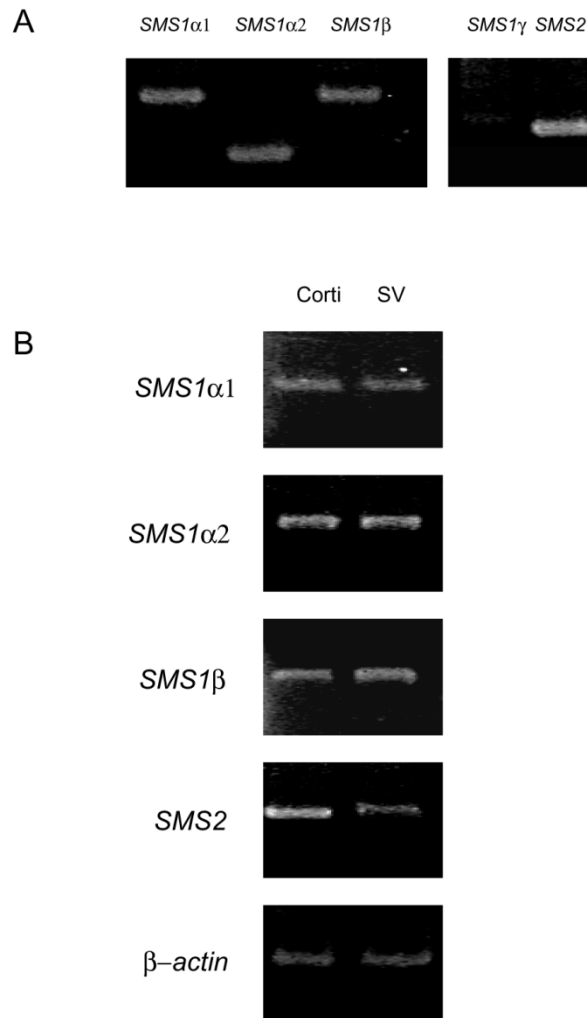


Fig. 3-1. Examination of *SMS1* variances and *SMS2* expression in mouse inner ear. These genes except for *SMS1γ* were found to be expressed in the inner ear (A) or in specific tissue like organ of Corti and the SV (B).

3.2 Identification of *SMS1*- and *SMS2*- deficient mice and their littermates

To know the genotypes of mice, we cut mice tail tips and extracted genomic DNA. PCR-based genotyping was performed using primer pairs that target either exon 2 or the neo cassette. As shown in Fig. 3-2, for both *SMS1*^{+/+} and *SMS2*^{+/+} mice, a single band with the least base pairs was obtained in all control mice, while a single band with the most base pairs was obtained in all KO mice. Both bands were

obtained in all heterogeneous mice.

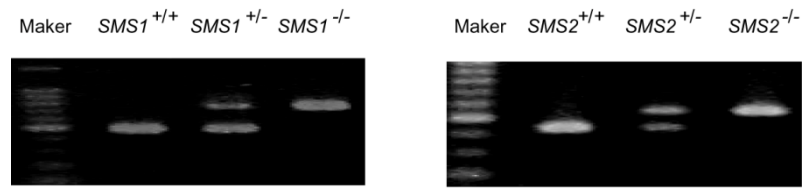


Fig. 3-2. Examination of genotype of newborn mice by PCR.

3.3 Behavioral tests

We first assessed the hearing ability of SMS1- and SMS2-deficient mice in a behavioral test in which a water reward was associated with tone pulses and the SPL of the tone was varied to test the detection threshold of the animal. The SPL was randomly selected to be in the range from 45 dB to 75 dB at 5 dB steps (7 levels, all referred to as S+). To find spontaneous licking rate (chance level), unrewarded trials in which neither acoustic stimuli nor water reward were presented (referred to as S-), were randomly intermingled with the rewarded trials. In *SMS1^{+/+}* mice, all levels of the S+ except for 45 dB induced licking behavior at a rate significantly more than during the S- trials (Fig. 3-3 A; $n = 7$, $p < 0.05$), suggesting that *SMS1^{+/+}* mice could hear the tone at a level of 50 dB or above in our experimental conditions. In the *SMS1^{-/-}* mice, however, only S+ presentations greater than 65 dB induced licking behavior at a rate significantly higher than that observed in the S- trials (Fig. 3-3 B; $n = 8$). In contrast, in *SMS2^{-/-}* mice, all levels of the S+ induced licking behavior at a rate significantly higher than that observed in the S- trials (Fig. 3-3 C; $n = 6$).

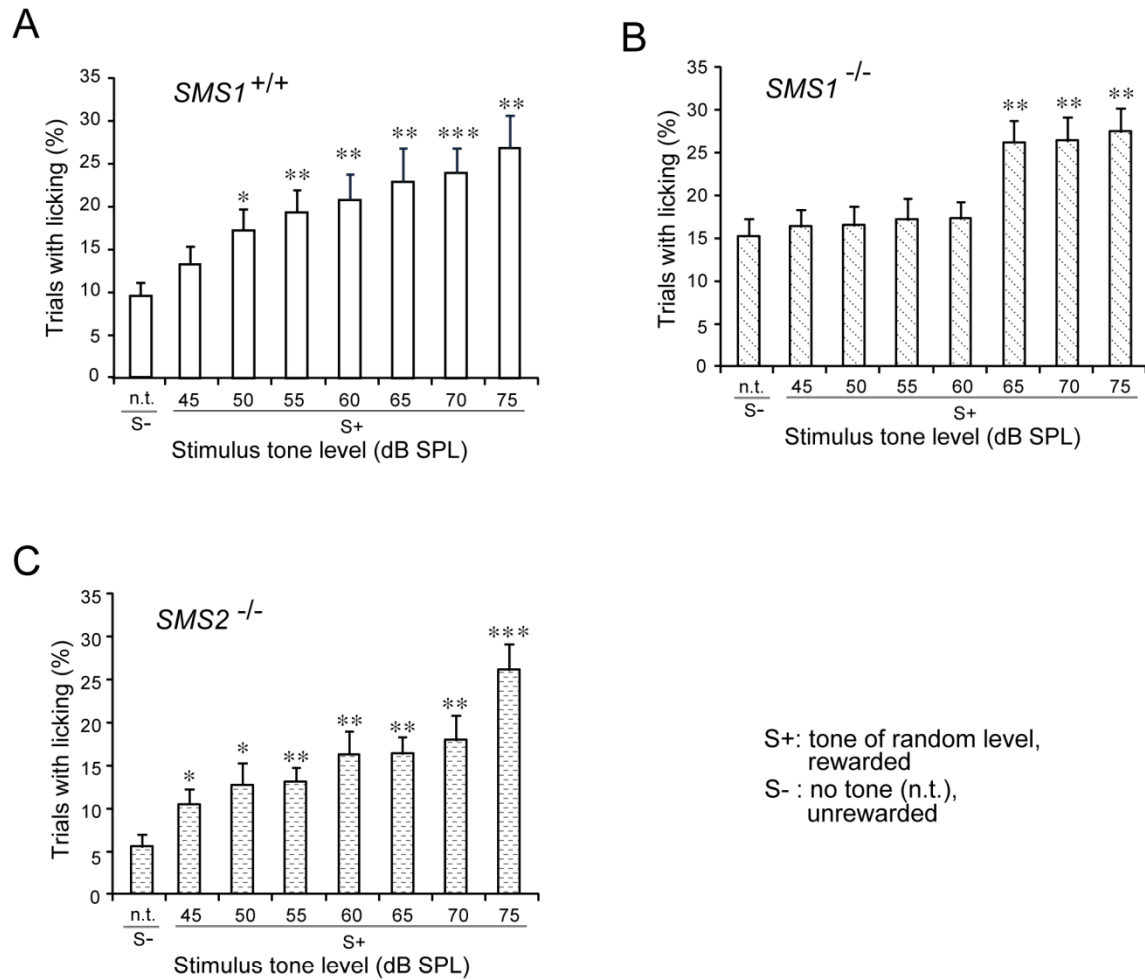


Fig. 3-3. Increase in the detection threshold of 4-kHz tones in 3-month-old *SMS1*^{-/-} but not *SMS2*^{-/-} mice. *A*, rates of exhibiting licking behavior within the trials in seven *SMS1*^{+/+} mice. The values were significantly higher than the chance level (S-) for all S+ stimulus levels except for 45 dB. *B*, rates of exhibiting licking behavior within the trials in eight *SMS1*^{-/-} mice. The values were significantly higher than the chance level only for tones at 65 dB or higher. *C*, rates of exhibiting licking behavior within the trials in six *SMS2*^{-/-} mice. The values were significantly higher than the chance level for all S+ levels. n.t. = no tone. Each bar represents the mean ± SEM. * = $P < 0.05$, ** = $P < 0.01$, *** = $P < 0.001$. Asterisk conventions apply to all figures.

3.4 ABR tests

The above behavioral results suggest that the hearing threshold of *SMSI*^{-/-} mice was elevated, whereas that of the *SMS2*^{-/-} mice was not. To further test hearing in these mice, we examined the ABR threshold using a click stimulus. As shown in Fig. 3-4 and Fig. 3-5 A, and in agreement with previous reports (Yoshikawa et al. 2009), ABRs in mice occurred 1-6 ms after stimulus onset. And the waveform has five peaks, peak I - V (Fig 3-4 A). Using a combination of ABR latency comparisons with near-field evoked potentials and lesion techniques, Henry (1979) concluded that the first peak had a cochlear origin, and the next four peaks corresponded to cochlear nucleus, contralateral superior olivary complex, lateral lemniscus, and contralateral lateral inferior colliculus, respectively. The ABR threshold was defined as the lowest SPL required to induce an ABR exceeding three times the SD of baseline noise (Fig. 3-4 B). As is clear from Fig. 3-5 A, the ABR threshold in the *SMSI*^{-/-} mouse was elevated compared to the threshold in the *SMSI*^{+/+} mouse. Fig. 3-5 B shows the ABR threshold results in *SMSI*^{-/-} animals at 1 month, 3 months, and 6 months of age and in *SMS2*^{-/-} mice at 3 months of age in response to click stimulus. The ABR threshold in the *SMSI*^{-/-} mice was significantly higher than that in age-matched *SMSI*^{+/+} littermates, at all ages ($p < 0.01$). There was also a clear elevation in ABR threshold in *SMSI*^{-/-} mice that were one to three months of age ($p < 0.01$). In contrast, *SMS2*^{-/-} mice had low ABR thresholds that were not significantly different from their *SMS2*^{+/+} control littermates ($p > 0.05$; Fig. 3-5 B, right end). These results support the notion that *SMSI*^{-/-} mice have hearing impairments, whereas *SMS2*^{-/-} mice do not, and they further suggest that there is an age-related progression of hearing loss in *SMSI*^{-/-} mice.

To test the frequency dependence of hearing loss in *SMSI*^{-/-} mice, we examined the ABR threshold with tones of different frequencies. As shown in Fig. 3-6 A-C, hearing impairments occurred at lower frequencies for all age groups tested. At 1 month of age, hearing loss was most prominent at 4 kHz, whereas at 3 and 6 months the most severe hearing loss occurred at 8 kHz (Fig. 3-6 A-C). We also examined the frequency dependency of the ABR threshold in *SMS2*^{-/-} mice, and again found no

differences from their *SMS2*^{+/+} control littermates at any frequency (Fig. 3-6 D), consistent with the observations using click stimulation.

The effect of genetic background is an important issue in hearing research. Indeed, a splice variant of the cadherin 23 gene (*Cdh23*) has been proved to affect early onset of hearing loss (Noben-Trauth et al. 2003). We generated the SMS1 KO mice using the D3 stem cells, and backcrossed with the C57BL/6 strain, a strain most frequently used in neuroscience research. But the C57BL/6 strain also carries the *Cdh23ahl* allele (Noben-Trauth et al. 2003). Thus all mice (*SMS1*^{-/-}, *SMS1*^{+/+}, *SMS2*^{-/-}, and *SMS2*^{+/+}) used in our study carry the *Cdh23ahl* allele. To identify the effect of SMS1- and SMS2-deficiency, we always compared the results in *SMS1*^{-/-} mice to their littermate *SMS1*^{+/+} mice (Fig. 3-6). We did find differences between wild type animals and *SMS1*^{+/+} mice at 3 months and 6 months (Fig. 3-6 B, C and D). These data suggest that factors other than *cdh23* mutation in the 129S2 strain affect hearing; such factors await to be clarified in future studies.

Because SM is also a component of axonal myelin sheath, one may expect changes in the conduction velocity of axons in the KO mice. As a rough estimation of conduction time, we measured the interval from the first peak to the fifth peak in the ABR waveform to click stimulation at 60 dB. The interval was 3.19 ± 0.12 ms in *SMS1*^{+/+} mice (n = 8), 3.32 ± 0.07 ms in *SMS1*^{-/-} mice (n = 9), 3.29 ± 0.04 ms in *SMS2*^{+/+} mice (n = 6), and 3.33 ± 0.06 ms in *SMS2*^{-/-} mice (n = 6) (all at 3 months of age). As shown in Fig. 3-5 C, no significant differences were found between these groups ($p > 0.05$).

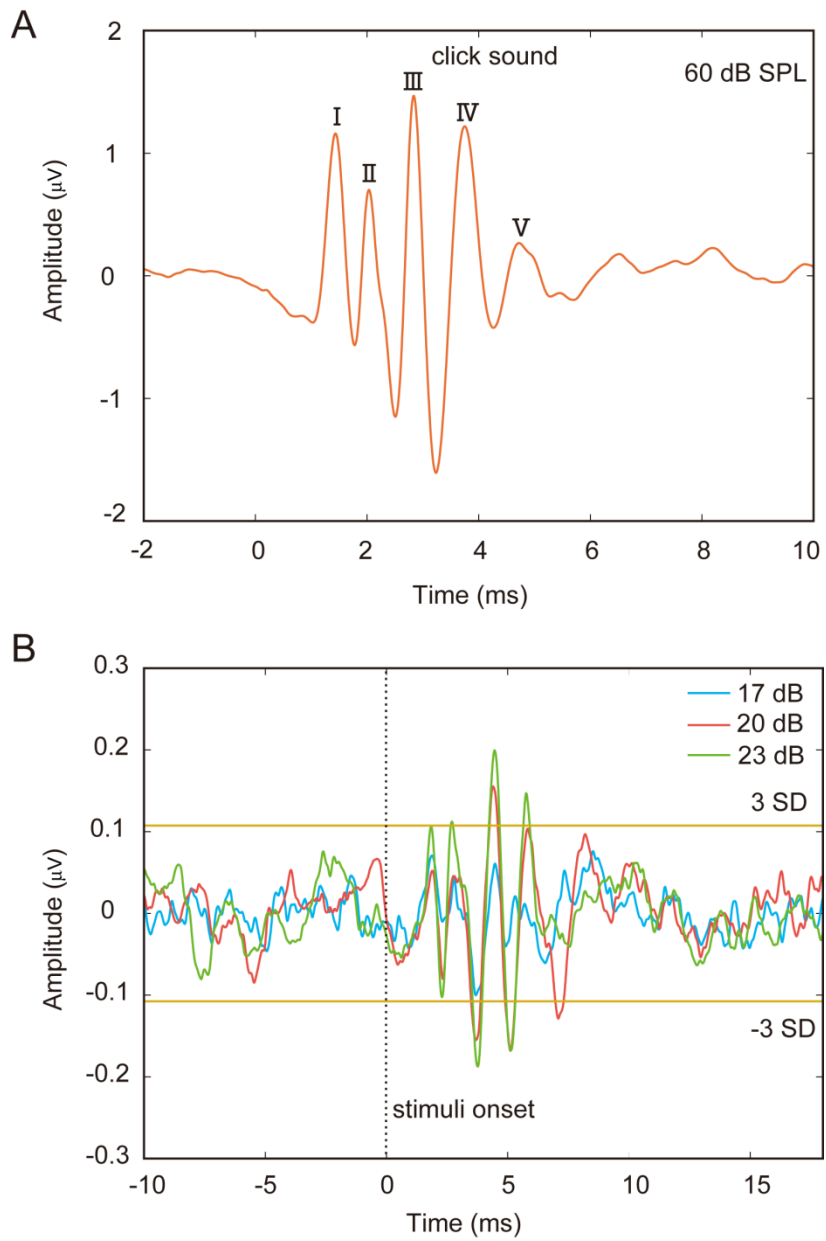


Fig. 3-4. Representative ABR waveform and definition of ABR threshold. A, ABR recording in response to a click stimulus at sound pressure level of 60 dB. I -V indicate the five peaks. B, the way to determine the response. The dotted line presents the stimuli onset time; SD presents standard deviation of baseline level (10 ms prior to sound stimuli). Both A and B are from an *SMSI*^{+/+} with the age of 3 months.

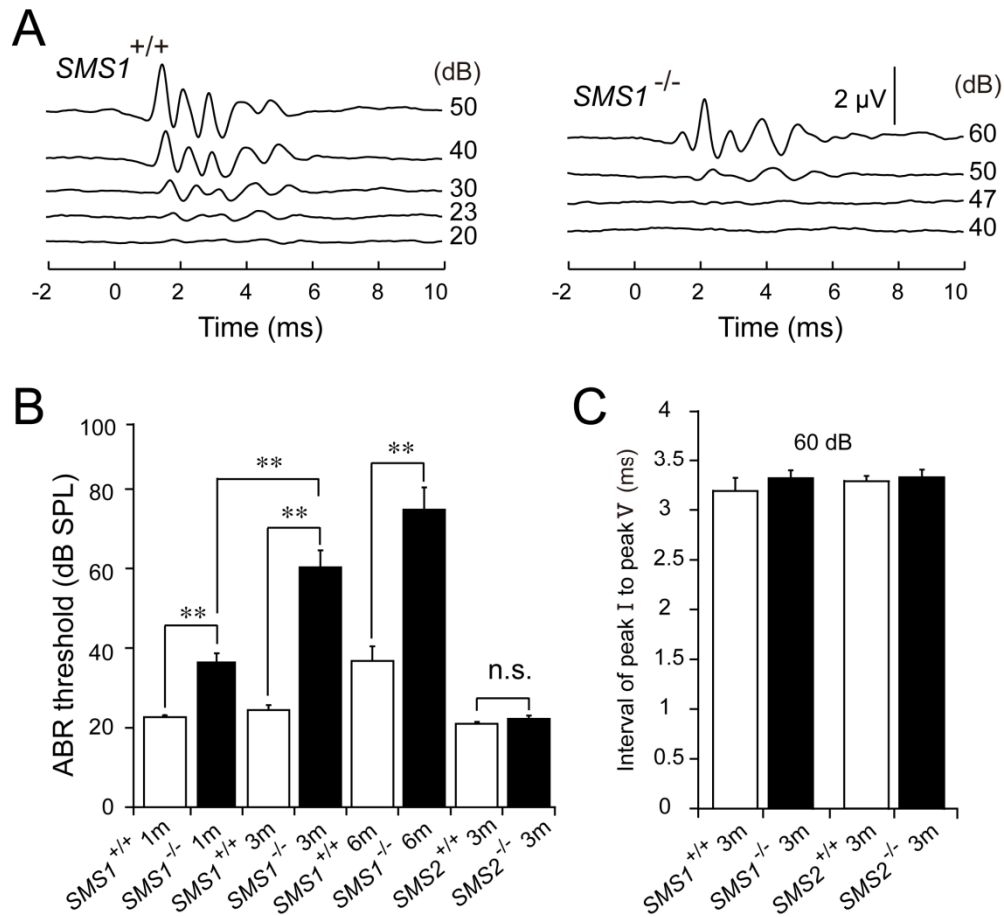


Fig. 3-5. ABR analyses in response to click sound. *A*, representative click-evoked ABR waveforms from an *SMS1*^{+/+} mouse (left trace group) and an *SMS1*^{-/-} mouse (right trace group), both at 3 months of age. The voltage calibration scale applies to all recordings. *B*, ABR thresholds in response to a click stimulus in 1-month-old *SMS1*^{+/+} mice ($n = 18$) and *SMS1*^{-/-} mice ($n = 14$), 3-month-old *SMS1*^{+/+} mice ($n = 19$) and *SMS1*^{-/-} mice ($n = 17$), 6-month-old *SMS1*^{+/+} mice ($n = 9$) and *SMS1*^{-/-} mice ($n = 6$), and 3-month-old *SMS2*^{+/+} mice ($n = 6$) and *SMS2*^{-/-} mice ($n = 6$). *C*, the interval from the first peak to the fifth peak in the ABR waveform to click sound at 60 dB. The conduction velocity was not significantly different between groups (*SMS1*^{+/+}: $n = 8$; *SMS1*^{-/-}: $n = 9$; *SMS2*^{+/+} and *SMS2*^{-/-}: $n = 6$). Values were presented as means \pm SEMs. ns: not significant.

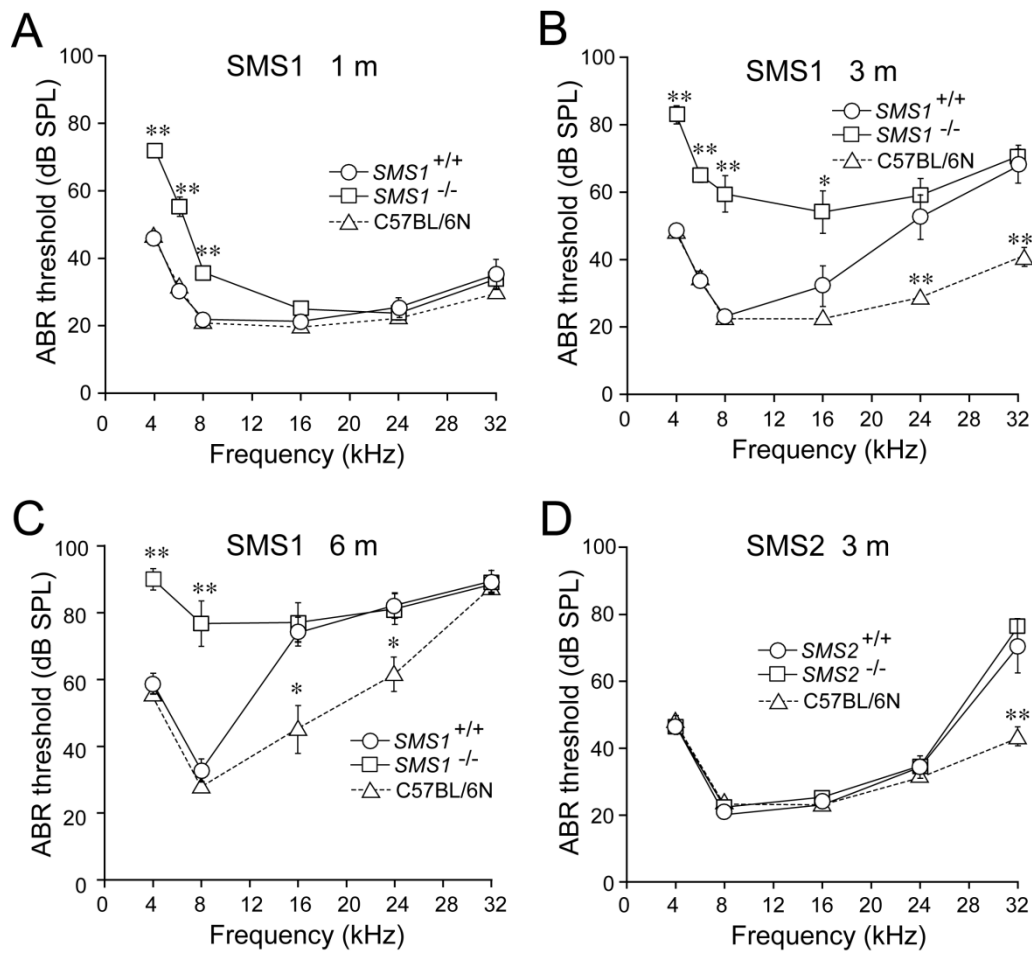


Fig. 3-6 Frequency-dependent ABR analyses. *A*, comparison of ABR thresholds in response to tones of different frequencies in 1-month-old *SMS1*^{+/+} mice (n = 4 for 6 kHz, n = 11 for other frequencies), and *SMS1*^{-/-} mice (n = 4 for 6 kHz, n = 9 for other frequencies). *B*, comparison of ABR thresholds in response to tones of different frequencies in 3-month-old *SMS1*^{+/+} mice (n = 4 for 6 kHz, n = 14 for other frequencies) and *SMS1*^{-/-} mice (n = 4 for 6 kHz, n = 12 for other frequencies). *C*, comparison of ABR thresholds in response to tones of different frequencies in 6-month-old *SMS1*^{+/+} mice (n = 9) and *SMS1*^{-/-} mice (n = 8). *D*, comparison of ABR thresholds in response to tones of different frequencies in 3-month-old *SMS2*^{+/+} mice (n = 6) and *SMS2*^{-/-} mice (n = 6). C57BL/6N wide type mice data were also added at each age (n = 6 at each age). ns: not significant. Values were presented as means ± SEMs.

3.5 Cochlear function in the KO mice

The elevation of the ABR threshold in *SMSI*^{-/-} mice means that the SPL required to induce the first peak of the ABR response, which reflects cochlear activity, was also elevated (see Fig. 3-5 A), and thus suggests dysfunction of the cochlea. Further, because *SMSI*^{-/-} mice were not deaf (Fig. 3-5), we suspected that mechanisms in the cochlea that enhance cochlear sensitivity may be impaired in these mice. We therefore first examined the EP and endolymph K⁺ concentration, and then otoacoustic emissions in the *SMSI*^{-/-} mice.

We used a double-barreled microelectrode to examine EPs and endolymph K⁺ concentrations at the same time (Fig. 2-7), in animals across different ages. We calibrated the microelectrode at 38 °C before and immediately after recording (see method). Table 3-1 and Fig. 3-7 show calibration values and fitting curves, respectively, from the same *SMSI*^{+/+} mouse at three months of age. In this animal, a potassium concentration of 148 mM was calculated according to the measured potassium potential and the fitting curve after recording.

As shown in Fig. 3-8 A, B and C, the EP in the *SMSI*^{+/+} control littermates had a value close to 100 mV (98.0 ± 4.5 mV, n = 10, at 1 month of age; 96.1 ± 5.5 mV, n = 8, at 3 months of age; 97.7 ± 6.7 mV, n = 12, at 6 months of age; no significant difference among these groups; p > 0.05), in agreement with previous reports in wild-type animals (Kitajiri et al. 2004; Yoshikawa et al. 2009). The EPs in *SMSI*^{-/-} mice at 1 month of age (79.7 ± 4.5 mV, n = 8), 3 months of age (65.5 ± 4.9 mV, n = 10), and 6 months of age (68.7 ± 4.5 mV, n = 8) were all found to be significantly reduced as compared to age-matched *SMSI*^{+/+} controls (Fig. 3-8 A, B and C; p < 0.01). The potentials in 3-month-old and 6-month-old *SMSI*^{-/-} mice were also significantly lower than that of the 1-month-old animals (Fig. 3-8 C; p < 0.01).

In accord with previous reports on wild-type animals (Kitajiri et al. 2004; Yoshikawa et al. 2009), the K⁺ concentration in the endolymph of *SMSI*^{+/+} mice was 144.4 ± 10.2 mM (Fig. 3-8 D; n = 11). The K⁺ concentrations in the endolymph of age-matched *SMSI*^{-/-} mice were found to have similar values (146.9 ±

9.0 mM, n = 9, p > 0.05; Fig. 3-8 D).

EPs in *SMS2^{-/-}* mice either at 1 month of age (98.0 ± 8.0 mV, n = 6) or at 6 months of age (95.4 ± 3.8 mV, n = 8) were not significantly different from those in the *SMS2^{+/+}* mice (97.3 ± 6.1 mV, n = 6 at 1-month; p > 0.05; Fig. 3-8 E). These EP values were also not significantly different from those in the *SMS1^{+/+}* mice (p > 0.05).

Next we examined otoacoustic emissions in the frequency range of 4 kHz to 29 kHz by fitting a probe to the ear canal. Fig. 3-9 A shows an example of a DPOAE measurement from a 3-month-old *SMS1^{+/+}* mouse. Application of two primary tones of frequencies f1 and f2 (f2/f1 = 1.22) induced distortion components of 2f1-f2, 3f1-2f2, and 4f1-3f2, among which the cubic component 2f1-f2 had the largest magnitude (Fig. 3-9 A). We compared the 2f1-f2 component measured at different frequencies in KO and control animals (Fig. 3-9 B). The component was significantly smaller in *SMS1^{-/-}* mice in the middle frequency range (8-16 kHz) than in their *SMS1^{+/+}* control littermates (p < 0.01, Fig. 3-9 B).

[K ⁺] (mM)	V _{before} (mV)	V _{after} (mV)	V _{5mM-[K⁺]_o} (mV)	V _{K⁺} (mV)	V _{measure}
5	40	40			
25	71.3	72.9			
50	82.0	87.4	7.1	66.2	40+7.1+
80	94.0	98.2			66.2=113.3
120	103.3	108.5			
160	112.5	116.3			

Table 3-1. An example of calibration values before and immediately after experiment from an *SMS1^{+/+}* mouse at 3 months of age. V_{5mM-[K⁺]_o} presents the potential difference between two conditions, when microelectrode is in the 5mM KCl solution and when the microelectrode is in the tissue fluid; V_{K⁺} presents the potassium potential; and V_{measure} presents the total K⁺ potential which equals the summation of V_{K⁺}, V_{5mM-[K⁺]_o} and the initial calibration value we set, in a KCl solution at 5 mM.

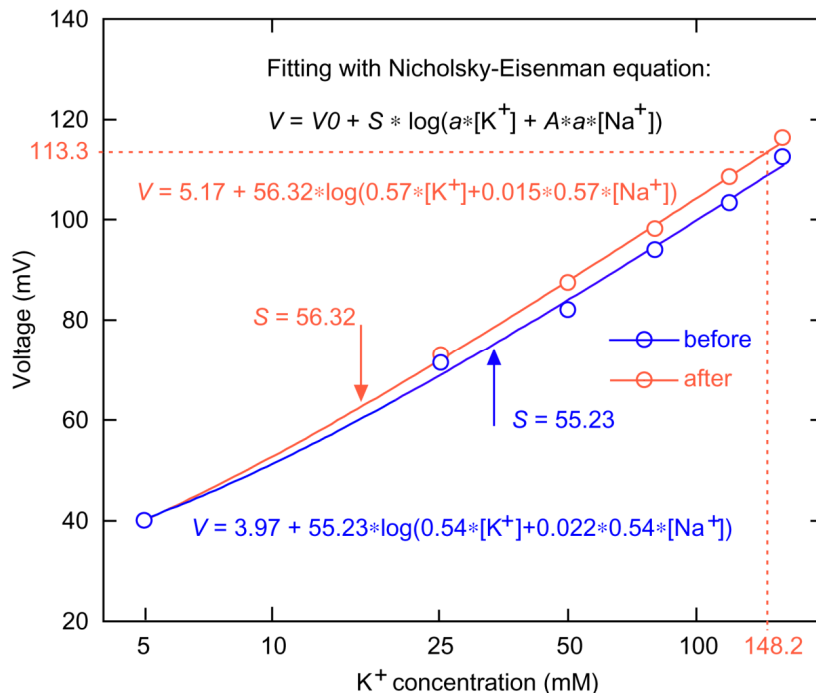


Fig. 3-7. An example of K^+ concentration calculation from the same $SMS1^{+/+}$ mouse at 3 months of age in Table 3-1. Red and blue cycles indicate the calibration values before recording and immediately after recording, respectively. The two curves indicate corresponding fitting to the cycles. The functions provided all parameters such as V_0 , A , and a . Before recording, the microelectrode has a slope of 55.23, while after recording it still show a very similar value of 56.23. The dashed lines show the potential measured and its corresponding potassium concentration calculated.

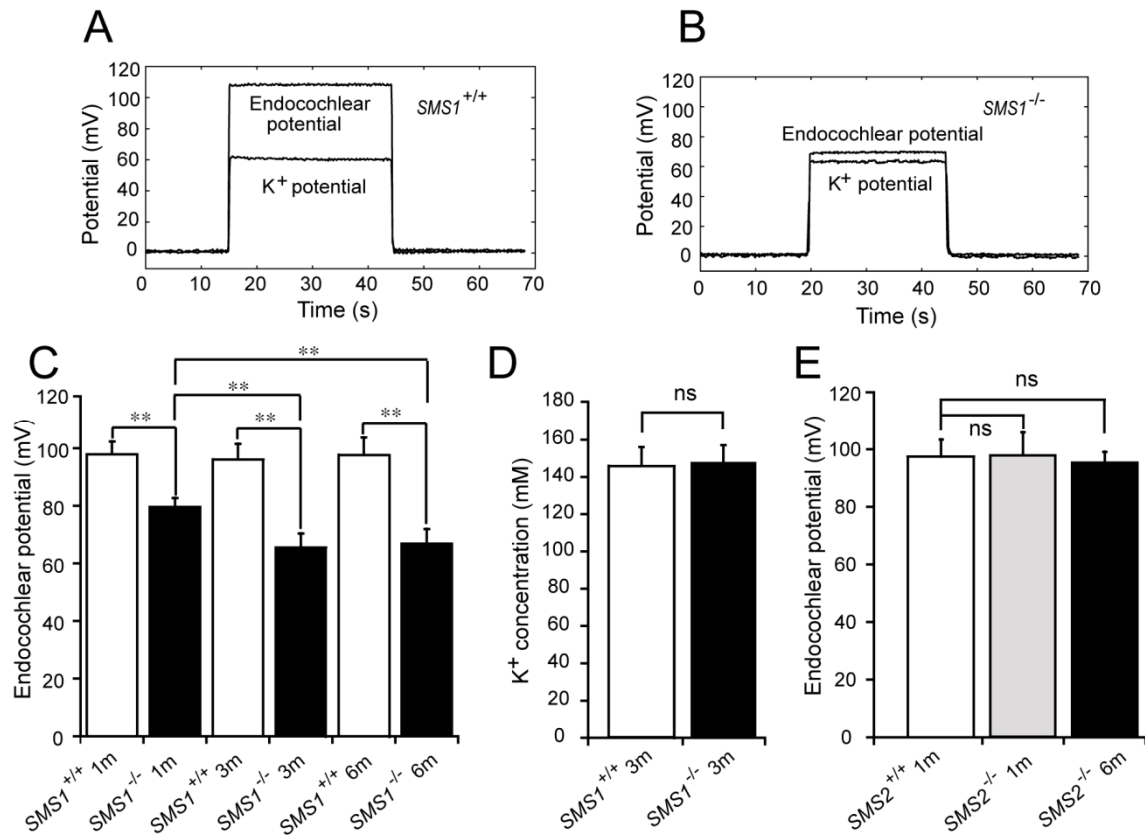


Fig. 3-8. Measurement of the EPs and endolymph K⁺ concentrations. *A* and *B*, representative recordings of EPs and PPs from the cochlea of an *SMS1*^{+/+} mouse and an *SMS1*^{-/-} mouse, both at 3 months of age. *C*, summary of EPs recorded from age matched *SMS1*^{+/+} and *SMS1*^{-/-} mice. *D*, comparison of K⁺ concentration in 3-month-old *SMS1*^{+/+} mice and *SMS1*^{-/-} mice. *E*, EPs in *SMS2*^{+/+} mice and *SMS2*^{-/-} mice. Values were presented as means ± SDs. ns: not significant.

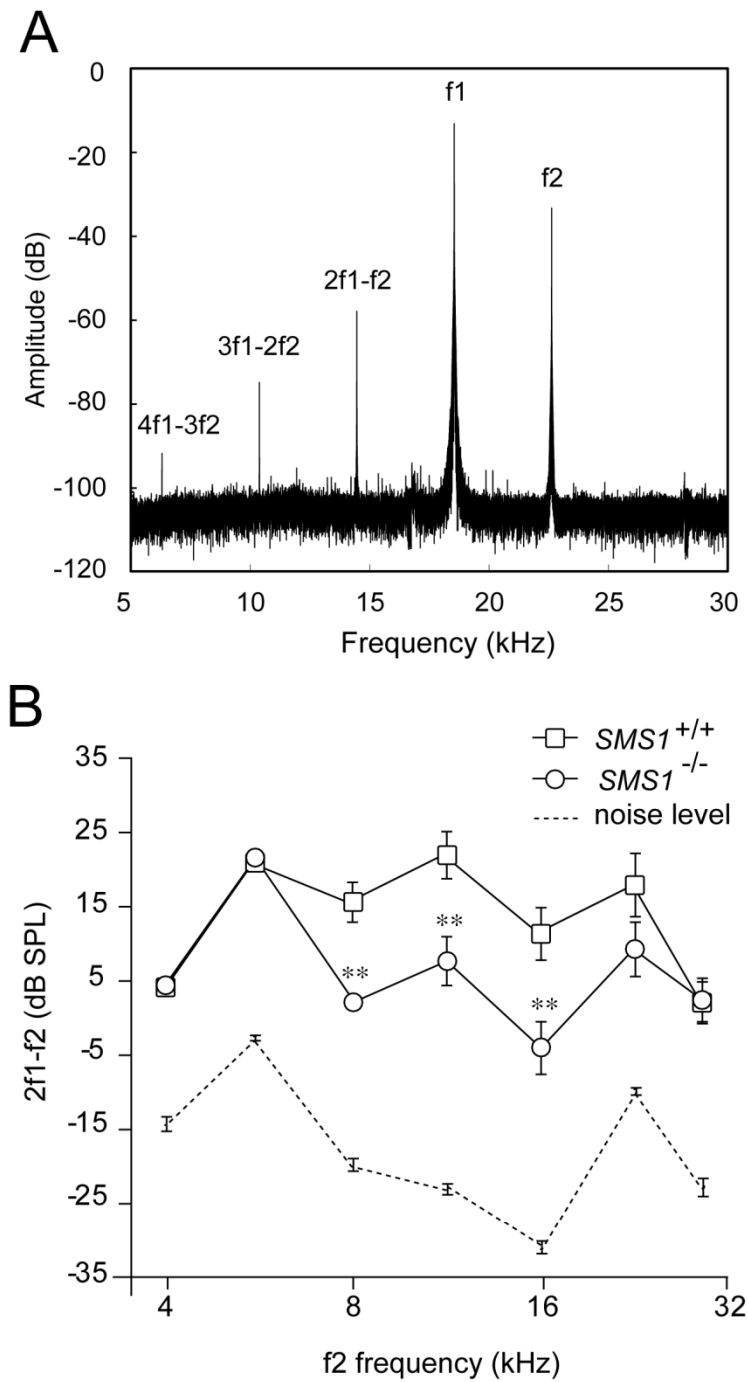


Fig. 3-9. DPOAE test results in *SMS1*^{+/+} and *SMS1*^{-/-} mice at 3 months of age. **A**, a representative DPOAE result from an *SMS1*^{+/+} mouse. **B**, frequency dependence of the 2f1-f2 component in 3-month-old *SMS1*^{+/+} mice (n = 12) and *SMS1*^{-/-} (n = 17) mice. Values were presented as means ± SEMs.

3.6 Cochlear histology

The smaller EPs in *SMSI*^{-/-} mice, as described above, suggest alterations in the cochlear SV of the *SMSI*^{-/-} mice because the SV is known to play a vital role in the generation of EPs (Wangemann, 2002; Hibino et al. 2010). Histological examination of the cochlea indeed revealed alterations in *SMSI*^{-/-} mice. Fig. 3-10 A and B show a hematoxylin and eosin-stained section through the middle turn of the cochlea in a 3-month-old *SMSI*^{+/+} mouse and an age-matched *SMSI*^{-/-} mouse, respectively. Although there was no clear change in the organ of Corti and the spiral ganglion, atrophy of the SV in the *SMSI*^{-/-} mouse was observed. As is clear from Fig. 3-10 B, the region towards the apical end and basal end appeared much thinner in *SMSI*^{-/-} mice compared with the *SMSI*^{+/+} controls (Fig. 3-10 B, arrow). Similar observations were obtained in all four *SMSI*^{-/-} mice when compared with six *SMSI*^{+/+} control littermates. Because previous studies have firmly established a place-frequency map in the mouse cochlea (Müller et al. 2005), we quantitatively examined SV atrophy at the apical, middle and basal turns of the cochlea to explore cochlear mechanisms for the frequency-dependent hearing loss in *SMSI*^{-/-} mice. The ends of SV appeared vague in cross sections (shown in Fig. 3-10 A and B), but the thickness of SV decreased rapidly towards both ends. We thus defined the ends of SV as the point at which SV thickness reduced to half of its maximum, and defined the width of SV (width in the base-to-apex direction) as the distance between the defined ends, along the SV surface. As shown in Fig. 3-10 C, the SV width was significantly shorter in *SMSI*^{-/-} mice than in their age-matched *SMSI*^{+/+} littermates, at all cochlear locations, and for both 3-month-old and 6-7-month-old animals. To test cochlear location-dependence, we normalized the SV width to the width of the lateral wall, measured between its two ends defined by the Reissner's membrane and the basilar membrane, respectively. As shown in Fig. 3-10 D, although the ratio was significantly smaller in the KO animals than their *SMSI*^{+/+} littermates at all cochlear locations and at both ages, we found no difference between cochlear locations. The reduction in the ratio in the KO animals was attributable to reduction in SV width, because the lateral wall width was independent of genotype (width

in μm in 3-month-old mice (mean \pm SD): apical: *SMSI*^{+/+} (286.4 ± 15.8 SD, n = 6), *SMSI*^{-/-} (299.2 ± 18.7 , n = 6), $p > 0.05$; middle: *SMSI*^{+/+} (361.5 ± 32.8 , n = 6), *SMSI*^{-/-} (362.5 ± 25.0 , n = 6), $p > 0.05$; basal: *SMSI*^{+/+} (445.7 ± 24.0 , n = 5), *SMSI*^{-/-} (445.8 ± 29.0 , n = 6), $p > 0.05$. 6-7-month-old: apical: *SMSI*^{+/+} (302.9 ± 9.8 , n = 4), *SMSI*^{-/-} (311.5 ± 7.9 , n = 5), $p > 0.05$; middle: *SMSI*^{+/+} (375.1 ± 5.6 , n = 4), *SMSI*^{-/-} (399.9 ± 11.6 , n = 5), $p > 0.05$; basal: *SMSI*^{+/+} (456.8 ± 20.0 , n = 4), *SMSI*^{-/-} (453.3 ± 17.8 , n = 5), $p > 0.05$).

In addition to the shrinkage of SV in the *SMSI*^{-/-} mice, F-actin staining with phalloidin revealed disorganization of marginal cells of the SV in *SMSI*^{-/-} mice. At the SV surface, phalloidin labels the tight junctions connecting marginal cells and thus reveals the shape and size of the apical membrane of individual marginal cells (Jabba et al. 2006). As shown in Fig. 3-10 E, marginal cells at the middle turn in the *SMSI*^{+/+} control animals exhibited polygonal shapes, but the size of the cells appeared rather uniform across the epithelium. In contrast, marginal cells in *SMSI*^{-/-} mice showed marked variation in their sizes (Fig. 3-10 F). Similar observations were made in five *SMSI*^{-/-} mice and five *SMSI*^{+/+} littermates. For a quantitative comparison, we measured apical membrane area size in both *SMSI*^{-/-} and *SMSI*^{+/+} mice using the NIH Image J software. The size in the control mice had a mean of $122.0 \mu\text{m}^2$ and an SD of $30.7 \mu\text{m}^2$ (210 cells from three animals), and the size in *SMSI*^{-/-} mice had a mean of $118.9 \mu\text{m}^2$ and an SD of $90.1 \mu\text{m}^2$ (239 cells from three animals). While the sizes in the control animals could be well fitted with a Gaussian function (Fig. 3-10 Ee2; $p < 0.05$, χ^2 test), the distribution of the sizes in *SMSI*^{-/-} mice was strongly skewed towards the right and could not be fitted with a Gaussian function (Fig. 3-10 Ff2; $p > 0.05$, χ^2 test), but could be approximated with a Rayleigh function with a scale parameter of 105.4 (Fig. 3-10 Ff2; $p < 0.05$, χ^2 test). Although we did not compare marginal cell size at different cochlear locations in a quantitative manner, the change in the KO animals appeared to be largely independent of cochlear location. At 6 months of age, although there was no obvious change in *SMSI*^{+/+} animals, marginal cell boundaries defined by phalloidin staining in *SMSI*^{-/-} mice became vague (data not shown).

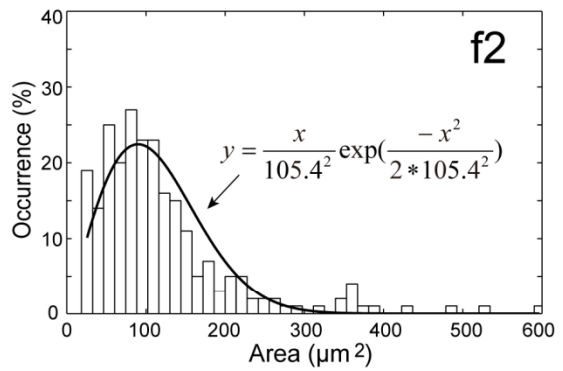
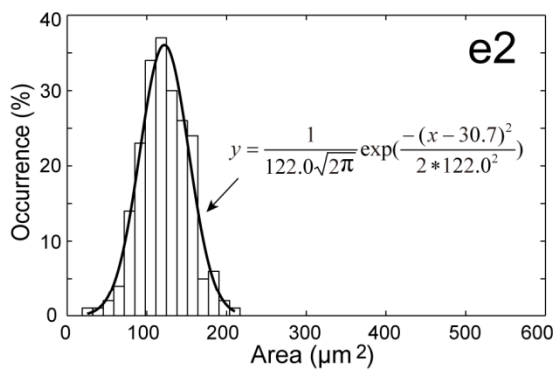
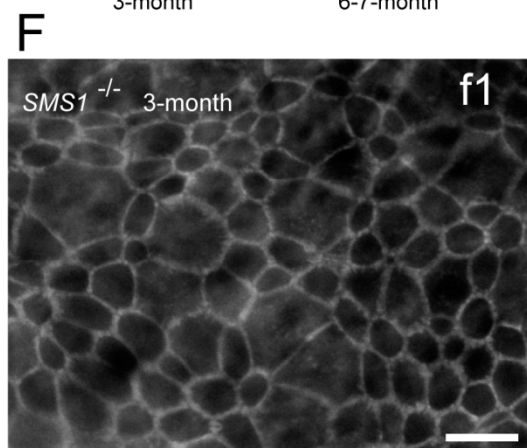
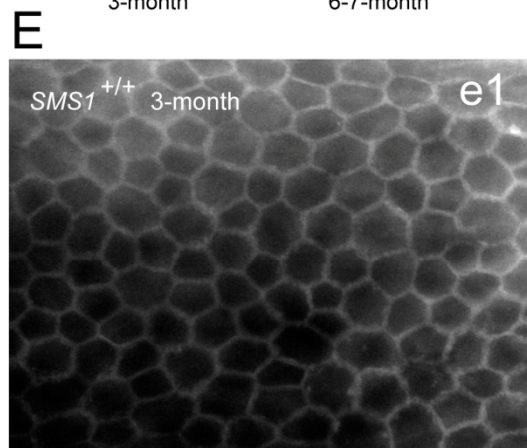
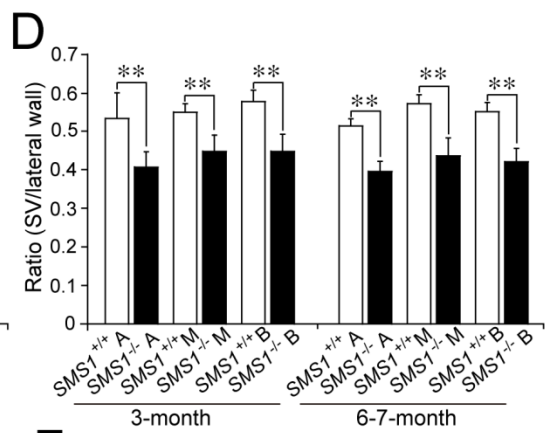
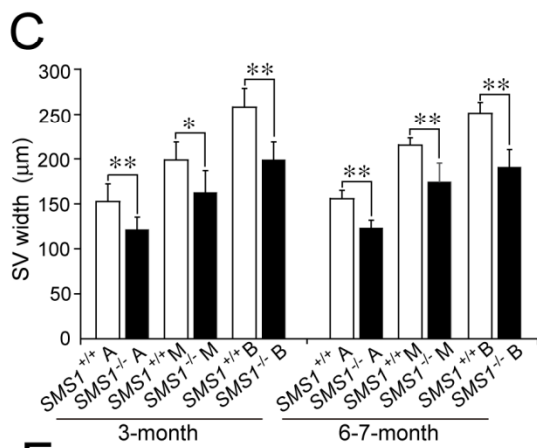
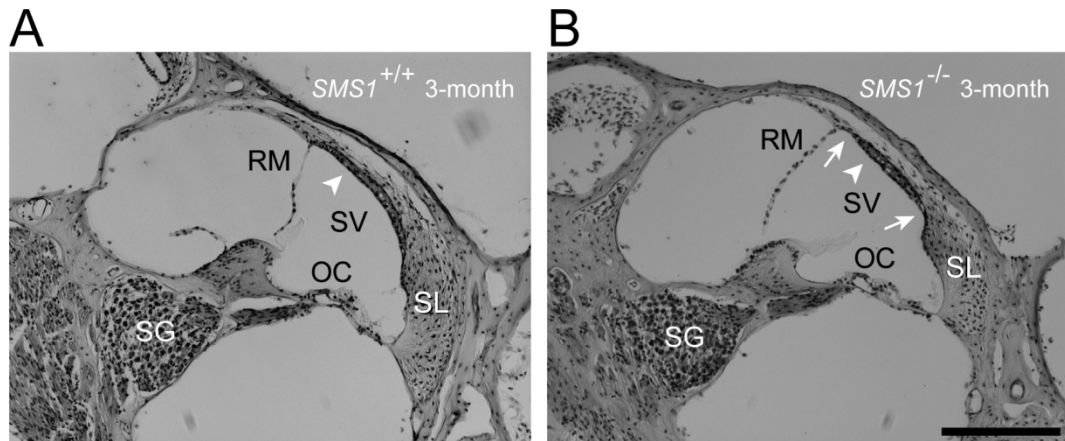


Fig. 3-10. Morphological abnormalities of the SV in *SMSI*^{-/-} mouse cochlea. *A* and *B*, hematoxylin and eosin stained cochlear sections at the middle turn in 3-month-old *SMSI*^{+/+} (*A*) and *SMSI*^{-/-} (*B*) mice. Arrowhead points to the SV. Note the shrinkage of the SV at the location indicated by the arrows in the *SMSI*^{-/-} mice (*B*). *C* and *D*, summary of SV width (*C*) and the ratio of SV width to lateral wall width (*D*) at the apical (*A*), middle (*M*), and basal (*B*) turns of cochleae from *SMSI*^{+/+} and *SMSI*^{-/-} mice at 3-months of age (n = 6 for each genotype), and at 6-7-months of age (*SMSI*^{+/+}, n = 4; *SMSI*^{-/-}, n = 5). *Ee1* and *Ff1*, phalloidin-stained strial marginal cells in flat-mount cochlear lateral wall preparations. *Ee2* and *Ff2*, histograms of marginal cell apical membrane area size in age-matched *SMSI*^{+/+} mice (*Ee2*, 210 cells from 3 animals) and *SMSI*^{-/-} mice (*Ff2*, 239 cells from 3 animals). The size in *SMSI*^{+/+} mice was fitted with a Gaussian function (*Ee2*, p < 0.05, χ^2 test), and the size in *SMSI*^{-/-} mice was fitted with a Rayleigh function (*Ff2*, p < 0.05, χ^2 test). Abbreviations: OC, the organ of Corti; RM, Reissner's membrane; SG, spiral ganglion; SL, spiral ligament. Scale bars: *B* = 0.2 mm = *A*; *Ff1* = 20 μ m = *Ee1*. Values are presented as means \pm SDs.

The cochlea receives its blood supply from a tight network of extremely slender vessels embedded in the highly compact bone of the otic capsule. The abundant blood vessel network facilitates the sufficient oxygen and nutrient to the cochlea. Normal blood supply to the cochlea is crucial to auditory transduction, the mechanism by which sounds are converted to nerve impulses that travel along the auditory pathways. Cochlear ischemia is followed almost immediately by hearing loss. Thus, we imaged the capillary network of the SV by isolectin staining. However, the blood vessels in *SMSI* KO mice were not significantly different from that in *SMSI*^{+/+} controls (Fig. 3-11).

The histological results described above may explain in part the reduction in EP, but do not appear to explain frequency-dependent hearing loss in *SMSI*^{-/-} mice. To further explore the mechanisms underlying the frequency-dependence of hearing loss in the KO mice, we stained the density of outer hair cells. The abnormalities of DPOAE in *SMSI*^{-/-} mice described in Fig. 3-9 also suggest alterations of the hair cells in

these animals. Loss of hair cells in *SMS1*^{-/-} mice, however, was limited, and we found no significant difference in outer hair cell density between *SMS1*^{-/-} mice and their *SMS1*^{+/+} littermates, at either the apical turn or the basal turn of the cochlea, and at either 3 months of age or at 6-7 months of age (Fig. 3-12).

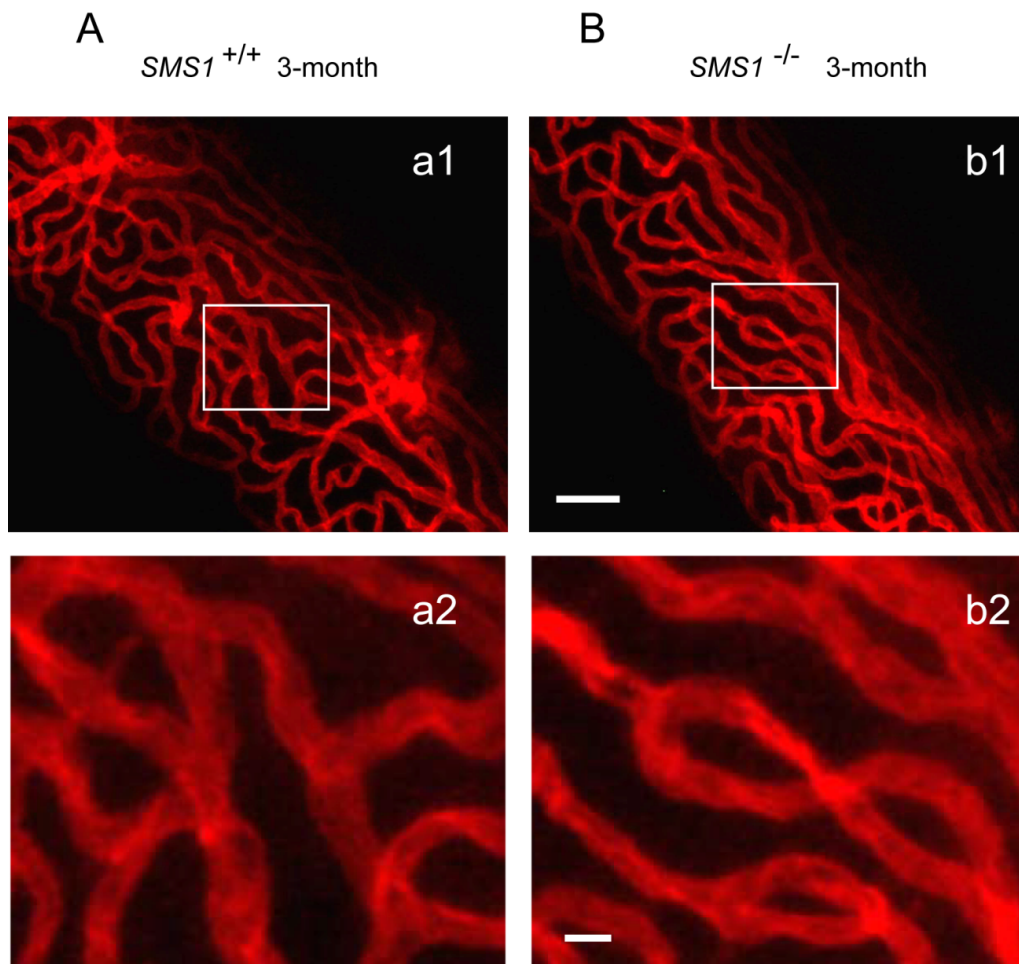


Fig. 3-11. Organization of capillaries in the SV. The SV capillaries were visualized by isolectin in an *SMS1*^{+/+} mouse (A) and an *SMS1*^{-/-} (B) mouse, both at 3 months of age. The lower panel a2 and b2 are enlarged views of the boxed area in a1 and b1, respectively. Scale bar: b1 = 50 μ m and also applies to a1; b2 = 10 μ m and also applies to a2.

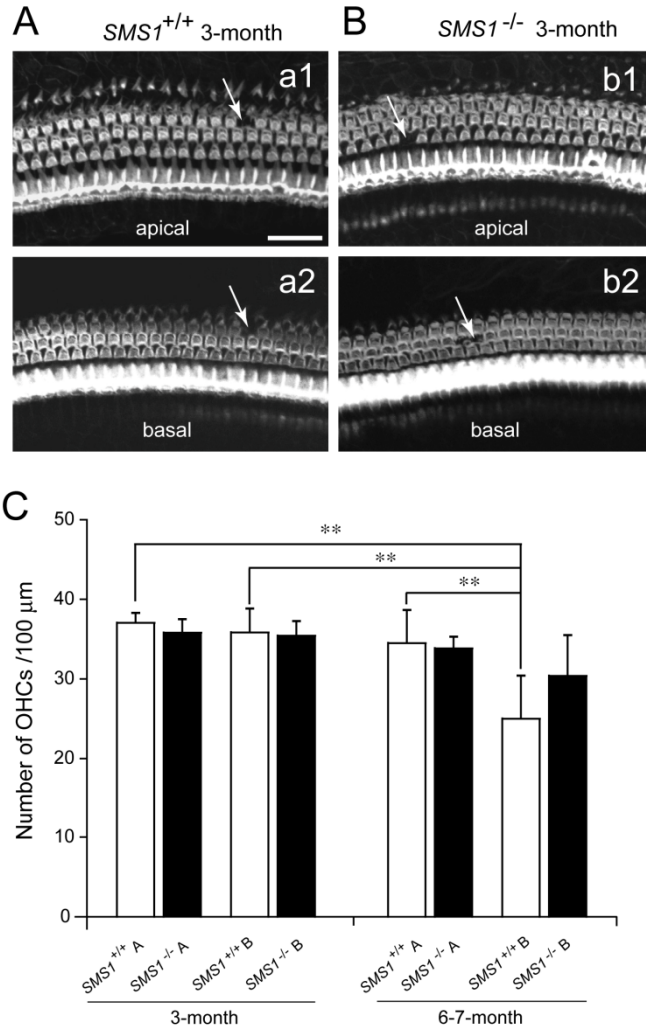


Fig. 3-12. Cochlear outer hair cell (OHC) density in *SMS1*^{-/-} mice was not significantly different from that in *SMS1*^{+/+} mice. *A*, representative phalloidin-stained OHCs at the apical (*a1*) and the basal (*a2*) turn from a 3-month-old *SMS1*^{+/+} mouse. *B*, OHCs from a 3-month-old *SMS1*^{-/-} mouse, shown in the same way as in (*A*). Arrows in (*A*) and (*B*) point to locations of OHC loss. *C*, summary of OHC density in *SMS1*^{+/+} and *SMS1*^{-/-} animals at 3-months of age (*SMS1*^{-/-} B, n=4; others, n = 5) and 6-7-months of age (*SMS1*^{-/-}A, n = 4; *SMS1*^{-/-}B, n = 3; others, n = 5). OHC density was defined as the total number of OHCs in all three rows of OHCs, per 100 μm length of the basilar membrane. *A* and *B* represent the apical and basal turn of the cochlea, respectively. Scale bar in (*A*) = 30 μm. Error bars are SEMs. No significant difference among non-labeled pairs.

3.7 KCNQ1 expression in the marginal cells of SV

The attenuated EPs in *SMSI*^{-/-} mice described above may, at least in part, account for the hearing impairments in these animals, and the abnormalities of the SV in *SMSI*^{-/-} mice may in part explain the attenuated EPs. To further explore the mechanism for the attenuated EPs in *SMSI*^{-/-} mice, we examined the expression of KCNQ1, a voltage-dependent potassium channel in the SV that plays an essential role in controlling EPs (Wangemann, 2002; Hibino et al. 2010). Immunostaining of KCNQ1 in the *SMSI*^{+/+} mice cochlea (3-month-old) revealed that the channel was expressed exclusively on the apical surface of marginal cells (Fig. 3-13 A, green), in accord with previous reports in wild-type animals (Sakagami et al. 1991; Jabba et al. 2006). Fig. 3-13 B shows the staining pattern in a 1-month-old *SMSI*^{+/+} mouse (Fig. 3-13 Bb1) and an age-matched *SMSI*^{-/-} mouse (Fig. 3-13 Bb2). It is clear from the figure that while staining in the *SMSI*^{+/+} mouse appeared rather continuous across the SV (Fig. 3-13 Bb1), some locations in the *SMSI*^{-/-} mouse appeared to be deprived of staining (Fig. 3-13 Bb2, arrowhead). In 3-month-old *SMSI*^{-/-} mice, more sites lacked staining (Fig. 3-13 Cc2, arrowheads). At this age, aberrant expression of the channel was also observed at locations other than the apical surface of marginal cells (Fig. 3-13 Cc2, arrows). In 7-month-old animals, the staining of KCNQ1 at the apical surface of *SMSI*^{-/-} mice marginal cells became only punctuate (Fig. 3-13 Dd2), and aberrant expression within the parenchyma of the SV (Fig. 3-13 Dd2, arrows) became comparable to that on the apical surface. Similar observations for each of the above age groups were obtained in all examined animals (1-month: *SMSI*^{+/+} n = 2, *SMSI*^{-/-} n = 2; 3-month: *SMSI*^{+/+} n = 6, *SMSI*^{-/-} n = 6; 6-7-month: *SMSI*^{+/+} n = 2, *SMSI*^{-/-} n = 3).

To examine cochlear location dependence and age dependence of KCNQ1 expression, we quantified the expression by measuring the width of the SV along the SV surface and the fraction of KCNQ1-positive length. As shown in Fig. 3-13 E, the fraction was close to one for all *SMSI*^{+/+} mice, but

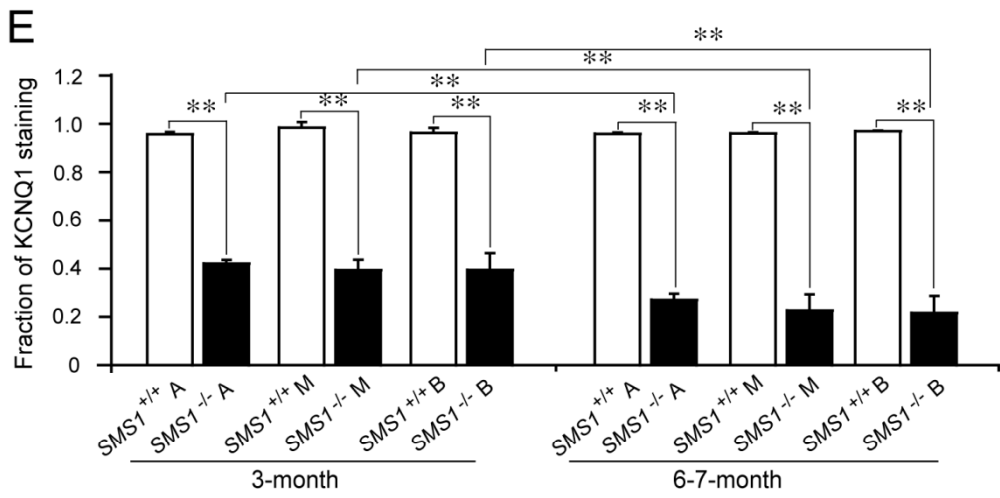
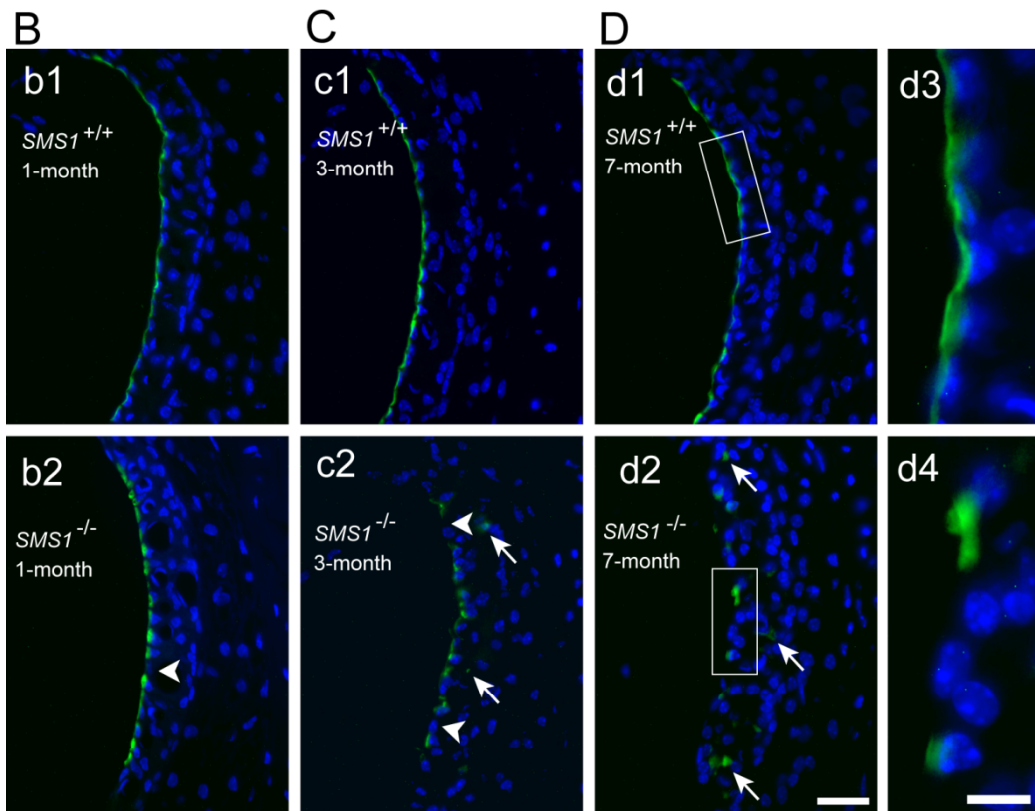
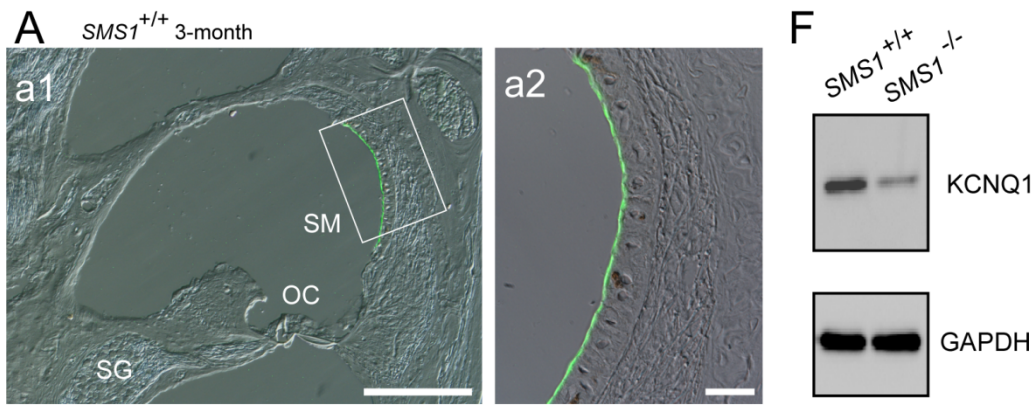


Fig. 3-13. Altered expression of KCNQ1 in the SV of *SMSI*^{-/-} mice. *Aa1*, specific expression of KCNQ1 in the SV in a 3-month-old *SMSI*^{+/+} mouse cochlear section. KCNQ1 immunofluorescence (green in the boxed area) was merged with a brightfield image of the section. *Aa2*, an enlarged view of the boxed area in *Aa1*. *B-D*, KCNQ1 immunostained SV sections of *SMSI*^{+/+} (*Bb1*, *Cc1*, *Dd1* and *Dd3*) and *SMSI*^{-/-} (*Bb2*, *Cc2*, *Dd2* and *Dd4*) mice at 1- (*B*), 3- (*C*), and 7- (*D*) months of age. KCNQ1 signals (green) were merged with images of DAPI-stained cell nuclei (blue). *E*, fraction of KCNQ1 staining along the SV surface in *SMSI*^{+/+} and *SMSI*^{-/-} animals at 3-months of age (n = 5 for all genotypes) and at 6-7-months of age (*SMSI*^{+/+}, n = 3; *SMSI*^{-/-}, n = 4). *A*, *M* and *B* represent apical, middle and basal turn of the cochlea, respectively. *F*, Western blot analysis for quantification of the KCNQ1 expression level in 3-month-old mice. Scale bars: *Aa1* = 0.2 mm; *Aa2* = 30 μm; *Dd2* = 30 μm and applies to *B*, *C* and *Dd1*; *Dd4* = 10 μm and applies to *Dd3*. Values were presented as means ± SEMs.

was significantly reduced in *SMSI*^{-/-} mice, at all cochlear locations. The results also revealed age-dependent reduction at all cochlear locations (Fig. 3-13 E). However, we found no significant difference *between* cochlear locations (Fig. 3-13 E).

To quantify the protein level of KCNQ1 in the SV, we performed western blot analysis. As shown in Fig. 3-12 F, the expression of KCNQ1 in 3-month-old *SMSI*^{-/-} mice was markedly reduced. The expression level of KCNQ1 normalized to the level of GAPDH expression, in *SMSI*^{-/-} mice was 60% of that in the age-matched control littermates (Fig. 3-13 F).

3.8 Pigmentation in the SV

Although the above analyses shed some light on the mechanisms underlying hearing loss in *SMSI*^{-/-} mice, the mechanism underlying the frequency-dependence of hearing loss remains elusive. Our previous study of *SMSI*^{-/-} mice demonstrated increased reactive oxygen species in these animals (Yano et al. 2011). In the cochlea, oxidative stress is known to induce macrophage invasion into the SV (Jabba et al. 2006, Singh & Wangemann, 2008). We thus examined macrophage invasion of the SV at different cochlear locations and at different ages. As shown in Fig. 3-14 A-D, macrophages were visible in transmission images of the SV by their pigmentation (Jabba et al. 2006), and there appeared to be more pigmentation in the KO animals. We quantified macrophage invasion by calculating the ratio of the area of pigmentation to the area of the SV, and found a significant enhancement at the apical turn in *SMSI*^{-/-} mice compared with *SMSI*^{+/+} littermates, but not at the basal turn, at 3 months of age (Fig. 3-14 E). There was also a tendency for more pigmentation at the apical turn than the basal turn in KO animals, at both 3 months of age and 6-7 months of age (Fig. 3-14 E).

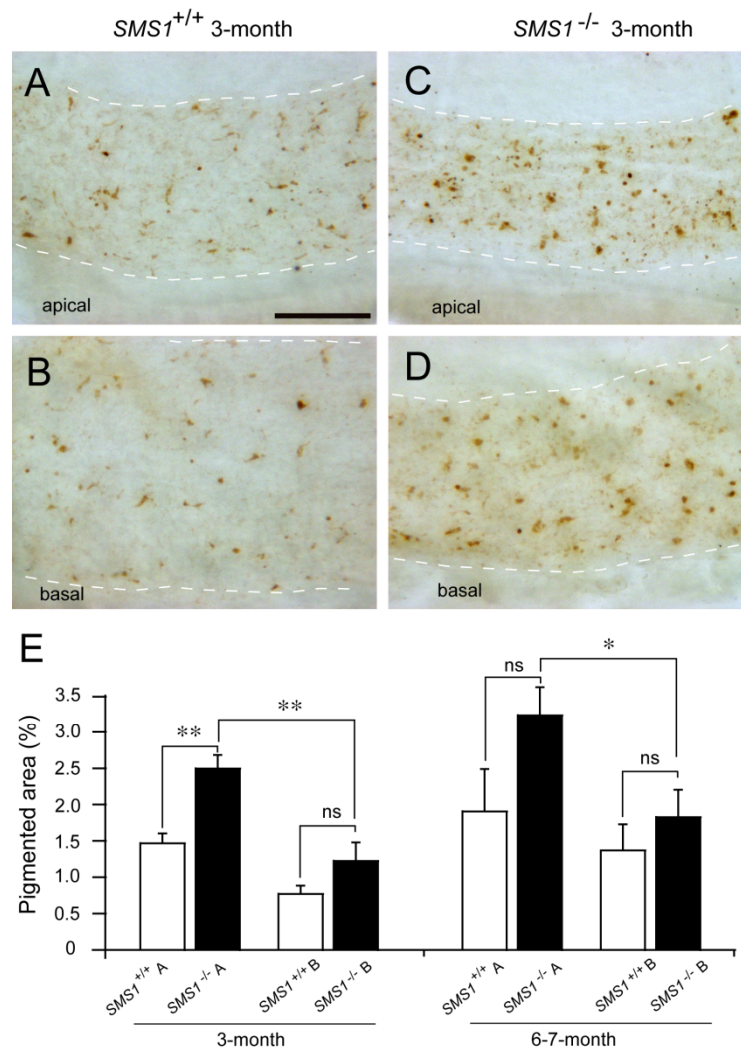


Fig. 3-14. Increased pigmentation in the SV of *SMS1*^{-/-} mice. A-D, brightfield microscope images of flat-mount tissues of the SV on the spiral ligament, prepared from 3-month-old *SMS1*^{+/+} (A, B) and *SMS1*^{-/-} (C, D) mice at the apical (A, C) and basal (B, D) turn of the cochleae. The SV could be identified as a pigmented stripe (the area between the two dotted lines in each figure). Pigment was accumulated more in the *SMS1*^{-/-} mice (C, D) than *SMS1*^{+/+} mice (A, B). Scale bar: 0.2 mm. E, the percentage of pigmented area to the area of the SV at the apical (A) and basal (B) turns of cochleae in *SMS1*^{+/+} and *SMS1*^{-/-} mice, at 3-months of age (n = 5 for both genotypes) and 6-7-months of age (*SMS1*^{+/+}, n = 5; *SMS1*^{-/-}, n = 4). Values were presented as means ± SEMs. ns: not significant.

3.9 Hearing repair

Previous study has demonstrated increased reactive oxygen species (ROS) in *SMSI*^{-/-} mice (Yano et al. 2011). Our present data that more macrophage invasion into SV was observed in the apical region than the basal region of the cochlea, suggested a role of cochlear location-dependent oxidative stress in producing the frequency-dependence of hearing loss in *SMSI*^{-/-} mice. These results led us to hypothesize that increased ROS generation seen in *SMSI*^{-/-} mice underlies the phenotypes seen in these mice and that treatment with anti-oxidants might rescue these conditions. To test this idea, we supplied the anti-oxidant NAC in animal drinking water when animal are at three weeks of age and then analyzed the hearing ability in NAC-treated *SMSI*^{-/-} mice at 3 month of age. The NAC water feeding period is about 70 days. As control, *SMSI*^{+/+} mice were also fed with NAC-containing water simultaneously, and there was no obvious change of ABR thresholds in *SMSI*^{+/+} mice treated with NAC compared with mice not treated (Fig. 3-15 A). The hearing ability of *SMSI*^{-/-} mice was not restored after treatment with NAC when tested using either a click sound (Fig. 3-15 A) or tones with different frequency, 4-32 kHz (Fig. 3-15 B).

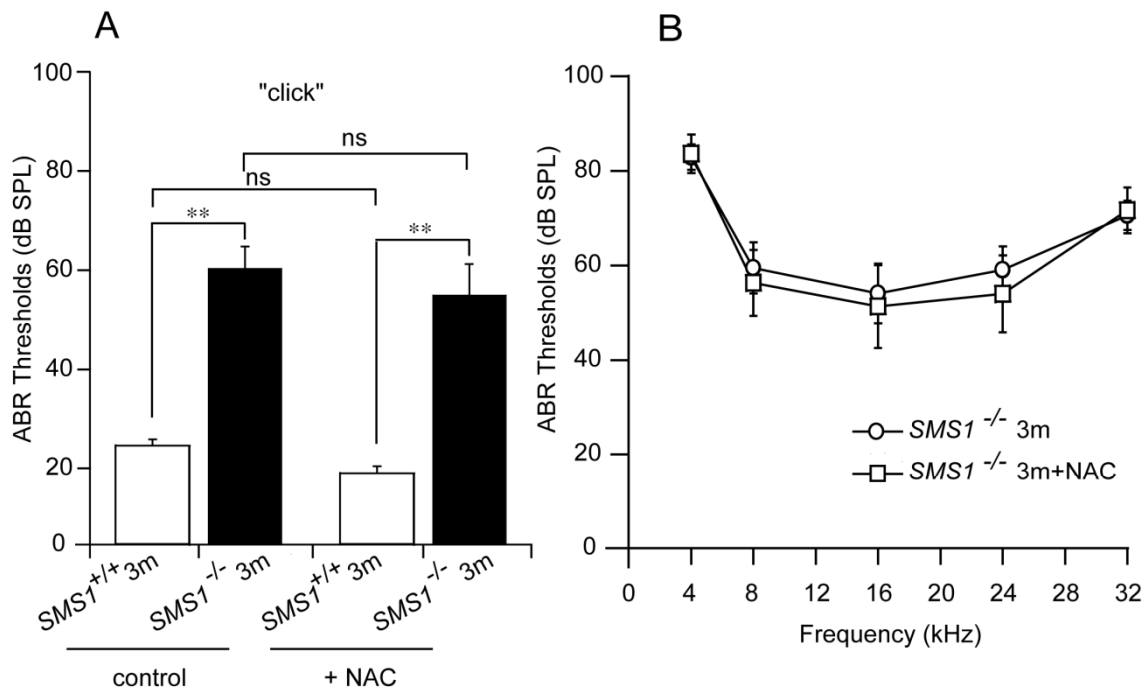


Fig. 3-15. Hearing repair test. A, ABR thresholds in control group mice (the same data in Fig. 3-5 B) and NAC-fed group ($n = 5$ for each) mice, in response to a click stimulus. **B,** the frequency-dependent ABR thresholds in $SMS1^{-/-}$ mice treated with NAC and in $SMS1^{-/-}$ mice not treated with NAC ($n = 5$ for each). Values are presented as means \pm SEMs. ns: not significant.

4 Discussion

In the present study, we demonstrated for the first time that hearing loss in *SMS1*^{-/-} mice, in a behavioral test that required detection of a tone at different levels and in ABR tests. *SMS2*^{-/-} mice, in contrast, showed no hearing loss either at the behavioral level or the electrophysiological level. We showed that the hearing loss in *SMS1*^{-/-} mice occurred in a low frequency range and was progressive with age. The results also demonstrated abnormalities in the inner ear of *SMS1*^{-/-} mice. Specifically, we found atrophy of the SV, disorganization of SV marginal cells, reduced EPs, altered expression of the potassium channel KCNQ1 in marginal cells, and a greater increase of macrophage invasion into the SV at the apical cochlea. In addition, a reduced level of DPOAE was observed in *SMS1*^{-/-} mice compared with *SMS1*^{+/+} littermates.

4.1 Hearing loss in *SMS1*^{-/-} mice, but not in *SMS2*^{-/-} mice

SM is an essential structural component of mammalian cell membrane (Tafesse et al. 2006), and is involved in the formation of lipid microdomains that play important roles in both protein sorting and signal transduction (Simons & Toomre, 2000; Helms & Zurzolo, 2004). It may thus not be a surprise that deficiency of the enzyme that synthesizes SM causes hearing impairments. An immediate question raised by our results is why hearing impairment was observed in *SMS1*^{-/-} but not *SMS2*^{-/-} mice. However, the explanation for this phenomenon is currently unclear. The results revealed that both SMS1 and SMS2 were expressed in the cochlea (see Fig. 3-2). Previous studies have also demonstrated the expression of both enzymes in the brain (Huitema et al. 2004; Yang et al. 2005), although the exact expression pattern of these enzymes in the auditory system is not known at this time. It is known, however, that whereas SMS1 resides in the membrane of the Golgi apparatus, SMS2 is primarily found in the cytoplasmic membrane (Huitema et al. 2004; Tafesse et al. 2006; Mitsutake et al. 2011; Kidani et al. 2012). SM

synthesis starts with the formation of ceramide in the endoplasmic reticulum, with ceramide being subsequently transported to the Golgi where SM is synthesized by SMS1. Furthermore, SM cycles between the Golgi and cytoplasmic membrane where SMS2 interconverts ceramide and SM (Tafesse et al. 2006). SMS1 thus appears to be essential to SM synthesis, whereas SMS2 plays only a regulatory role (Yamaoka et al. 2004). Such differential roles of SMS1 and SMS2 and their differential sub-cellular localization should serve as clues for further investigating why different phenotypes of KO animals were observed here. Despite normal hearing ability, *SMS2*^{-/-} animals were recently found to exhibit alterations both at the molecular and tissue level in a number of organs (Liu et al. 2009; Gowda et al. 2011; Li et al. 2011; Mitsutake et al. 2011; Zhang et al. 2011).

It is also interesting that not all cell types are impaired equally in *SMS1*^{-/-} mice. In this regard, although SV marginal cells were severely affected, other cells in the inner ear appeared to be less affected. The endolymph K⁺ concentration in the *SMS1*^{-/-} mice was not altered at all. Thus, the impact of SMS1-deficiency on cell functions appears to be cell type-dependent.

4.2 Features of the hearing impairment in *SMS1*^{-/-} mice

The results revealed several characteristic features of hearing impairment in *SMS1*^{-/-} mice. First, the impairment was more prominent for low frequency tones. Although our behavioral experiments used only a single frequency of 4 kHz, tests in the range of 4-32 KHz in the ABR experiments clearly demonstrated a greater impairment in the low frequency range. Second, compared to the hearing impairments in mice deficient of other lipid-related enzymes, the impairment in *SMS1*^{-/-} mice was mild to moderate. For example, the largest increase in the ABR threshold in *SMS1*^{-/-} mice was 40-50 dB as compared to the control mice (see Fig. 3-5). Mice genetically devoid of ganglioside synthase, in contrast, have complete hearing loss (Yoshikawa et al. 2009). Third, the impairment was progressive with age. Evidence from the ABR experiments, the EP recordings, and the KCNQ1 staining is all suggestive of an age-dependent

progression of hearing impairment in *SMS1*^{-/-} mice.

It is now well known that a mutation of the cadherin 23 gene (*Cdh23*), increases the susceptibility of early onset of age-related hearing loss (Noben-Trauth et al. 2003). Our *SMS1*- and *SMS2*-KO mice were generated using D3 stem cells, which originate from a 129 substrain, backcrossed with the C57BL/6 strain; both strains carry the *Cdh23ahl* allele (Noben-Trauth et al. 2003). Thus a possible effect of *Cdh23ahl* allele on the early onset and progressive nature of the hearing loss in *SMS1*^{-/-} mice must be considered. Among cochlear cell types, hair cells and cells of the Reissner's membrane are known to express cadherin 23 (Lagziel et al. 2005; Rzadzinska et al. 2005), raising the possibility of interaction between *SMS1* and cadherin 23 in these cells. Nevertheless, for the following reasons, the hearing loss we observed in *SMS1*^{-/-} mice appears primarily attributable to *SMS1*-deficiency. First, the hearing loss in *SMS1*^{-/-} mice was observed by comparison with their *SMS1*^{+/+} littermates. Second, *Cdh23ahl* allele-related hearing loss occurs in high frequency ranges (Kane et al. 2012), in contrast to the hearing loss in low frequency ranges in *SMS1*^{-/-} mice observed here. Third, *Cdh23ahl* allele-related hearing loss is caused by a loss of hair cells (Kane et al. 2012), but here we observed no significant difference in hair cell loss between *SMS1*^{-/-} and *SMS1*^{+/+} mice. Rather, abnormalities in the SV of *SMS1*^{-/-} mice appeared to be the primary mechanism for hearing loss. Finally, *Cdh23ahl* allele-related hearing loss starts from approximately 3 months after birth (Kane et al. 2012), but hearing loss in *SMS1*^{-/-} mice was observed here from the first month.

4.3 Mechanisms for hearing loss in *SMS1*^{-/-} mice

Our results suggest that atrophy of the SV may, at least in part, account for the hearing impairment in *SMS1*^{-/-} mice. Reduction of the thickness of the SV at the region close to the Reissner's membrane, and the disorganization of the marginal cells may all result in the attenuated EPs in these animals. EPs add to the driving force for K⁺ ions to enter hair cells through mechano-electrical transduction channels that are

activated upon acoustic stimulation. Loss of the EP thus reduces the sensitivity of hair cells to sound stimulation and leads to hearing impairments. The observation that the progressive reduction in the EPs paralleled the ABR threshold elevation (compare Fig. 3-8 C to Fig. 3-5 B) also argues for a causal role for EP attenuation in the hearing loss of *SMSI*^{-/-} mice.

To explore the mechanisms for the attenuated EPs in *SMSI*^{-/-} mice, we measured endocochlear K⁺ concentrations, but we found no significant changes. Instead, we found that KCNQ1 channels, which are normally expressed on the apical membrane of all marginal cells, were not expressed in some cells that face the scala media in *SMSI*^{-/-} mice. Moreover, in these mice, aberrant expression of KCNQ1 was found in the parenchyma of the SV, presumably on the processes of marginal cells within the stria. At the tissue level, the expression level of KCNQ1 was also low in *SMSI*^{-/-} mice. KCNQ1 normally passes K⁺ from the cytoplasm of marginal cells to the endolymph (Wangemann, 2002; Hibino et al. 2010). The major component of the EP is created by the low K⁺ concentration in the intrastrial space, the extracellular space confined by the two epithelial barriers of marginal cells and basal cells of the SV, both of which are formed by cells interconnected with tight junctions (Wangemann, 2002; Kitajiri et al. 2004; Hibino et al. 2010). The K⁺ concentration in the intrastrial space is regulated by ion channels, pumps, exchangers, and transporters of both the marginal cells and the basal cells (Wangemann, 2002; Hibino et al. 2010). Aberrant and reduced expression of KCNQ1 in the marginal cells of *SMSI*^{-/-} mice may have caused an increase of K⁺ concentration in the intrastrial space, leading to attenuated EPs. Hearing impairments resulting from loss of KCNQ1 channels in SV have also been shown before in mice deficient of the lysosomal membrane protein LIMP2 (Knipper et al. 2006), and mutations in the gene coding KCNQ1 α -subunit have been shown to cause deafness (Neyroud et al. 1997). The involvement of other molecules such as Cl⁻ channels and Cl⁻ transporters remains to be investigated in future studies (Rickheit et al. 2008).

It remains unclear whether the attenuation of the EP is cochlear location-dependent, and whether it explains the frequency-dependence of the hearing in *SMSI*^{-/-} mice. We measured EPs from only one site in the endolymph because the mouse cochlea is too small to allow measurement at different locations. EPs are determined not only by KCNQ1 channels, but other channels such as KCNJ10 and the Na⁺/K⁺ pump also play essential roles in creating the potential (Wangemann, 2002; Hibino et al. 2010). Previous studies have demonstrated oxidative stress-induced loss of KCNJ10 in the SV (Jabba et al. 2006; Singh & Wangemann, 2008). In light of the current observation that the apical region of *SMSI*^{-/-} mouse cochlea was more invaded by macrophages than the basal region (see Fig. 3-14), it is possible that the expression of EP-related molecules other than KCNQ1 but including KCNJ10, Cl⁻ channels and Cl⁻ transporters (Rickheit et al. 2008) is altered more in the apical region and causes a greater drop in the EP.

To explore the mechanism for the frequency-dependence of the hearing impairment, we measured DPOAE. However, DPOAE in the *SMSI*^{-/-} mice was reduced at a middle frequency range of 8–16 kHz. DPOAE is a nonlinear phenomenon, and is expected to be produced by active processes within the cochlea. It now appears to be attributable to the somatic motor of outer hair cells and the hair bundle motor of likely both inner and outer hair cells (for reviews see Dallos & Fakler 2002, Kemp 2002, Fettiplace & Hackney 2006, and Ashmore 2008), with the prestin protein and mechano-electrical transduction channels playing key roles in the somatic motor and hair bundle motor, respectively. Although our DPOAE results do not fully explain the frequency-dependence of hearing loss in *SMSI*^{-/-} mice (in particular the hearing loss at 4 kHz and 6 kHz judging from the ABR results), the results do suggest functional impairment of outer/inner hair cells in these mice. The fact that our EP and DPOAE results cannot fully explain the hearing loss in the *SMSI*^{-/-} mice, suggests that there may be additional impairments of the apical region of the cochlea in these mice. Such impairment might be caused by oxidative stress, considering our observation that macrophage density was more enhanced in the apical region than the basal region in *SMSI*^{-/-} mice.

Another feature of the hearing impairment in *SMS1*^{-/-} mice is its age-dependent progression. It is widely known that age-dependent development of hearing loss occurs in wild-type animals, but such hearing loss appears to be accelerated in *SMS1*^{-/-} mice as compared to *SMS1*^{+/+} littermates (see Fig. 3-5 B). The mechanism for age-dependent hearing loss is, at least in part, attributable to oxidative stress that impairs cell function or induces cell death (Staecker et al. 2001; Jiang et al. 2007). We have recently shown that mice genetically devoid of SMS1 exhibited increased reactive oxygen species (Yano et al. 2011). Although we found no obvious cell loss in *SMS1*^{-/-} mouse cochlea up to an age of 7 months, the accelerated progression of hearing loss in these mice may have been caused by increased oxidative stress. This notion is consistent with our observation that macrophage density in *SMS1*^{-/-} mouse cochlea tend to be higher than in *SMS1*^{+/+} controls. We also tried to rescue the hearing loss using the NAC. Unfortunately, the hearing ability was not restored in SMS1 deficient mice, but the ABR threshold in these NAC-treated KO mice was not significantly decreased compared with KO mice without NAC treatment. Firstly, this can be explained by tissue-specific ROS. Different tissue of these KO mice may suffer from ROS to a varying degree. Another possibility is the short time treatment with NAC. In previous study, we analyzed the ROS of pancreas in SMS1 KO mice after feeding the animal with NAC-containing water for 20-24 weeks (Yano et al. 2011). In the present study, the NAC treatment period only lasted 10 weeks, because by this time these KO mice were 3 months old and suffered from an accelerated progression of hearing loss. In addition, these mice showed larger individual difference among animals so that it makes the hearing assessment inaccurate by small samples.

It is unclear how SMS1 deficiency may lead to down regulation of KCNQ1 in marginal cells. At this time, one can only speculate on this issue. One possibility is the involvement of the cytoskeleton and the membrane lipid microdomain. In the present study, the down regulation of KCNQ1 channels was associated with disorganization of marginal cells. There is ample evidence demonstrating a close relationship between SM/ceramide and the cell skeleton (Meivar-Levy et al. 1997; Lenne et al. 2006;

Zeidan et al. 2008). We have previously shown that SM is reduced and ceramide is increased in the pancreatic islets of *SMS1^{-/-}* mice (Yano et al. 2011). Similar changes may occur in the SV of *SMS1^{-/-}* mice, although this remains to be clarified. On the other hand, SM and ceramide are important components of membrane lipid microdomains (Merrill, 2002; Tafesse et al. 2006). Reduced SM and the accumulation of ceramide, if it occurred in the *SMS1^{-/-}* mouse SV, could change the cytoskeleton and membrane lipid microdomain and consequently affect protein trafficking and signal transduction in the marginal cells of these animals (Hannun & Obeid, 2002; Merrill, 2002, Spiegel & Milstien, 2002; Subathra et al. 2011). Eventually, this could lead to deepithelialization of a portion of the marginal cells and the aberrant and reduced expression of KCNQ1 that we observed. Dysfunction of cochlear hair cells as suggested by the reduced level of DPOAE in the *SMS1^{-/-}* mice may also be caused by alterations of cytoskeleton or membrane stiffness (Oghalai et al. 1998; Zeidan et al. 2008; Tafesse et al. 2006). Other possibilities for the down regulation of KCNQ1 channel in *SMS1^{-/-}* mice may involve oxidative stress or protein degradation. Ceramide has been shown to down regulate HERG K⁺ channels by overproduction of reactive oxygen species (Bai et al. 2007) or by ubiquitin-mediated lysosomal degradation (Chapman et al. 2005). One could speculate that ceramide accumulates in *SMS1^{-/-}* mouse SV and down regulates KCNQ1 in marginal cells via similar mechanisms.

In summary, our results show for the first time that SMS1 but not SMS2 is involved in hearing, and that SMS1-deficiency causes progressive hearing loss at a low frequency range. Our results show an essential role of SMS1 for SV homeostasis, and suggest the involvement of an SMS1-related pathway in the regulation of the SV KCNQ1 channel. Future studies should elucidate the mechanisms underlying the differential roles of SMS1 and SMS2 in hearing, and examine the link between SM metabolism and frequency-dependent hearing at the molecular level.

5 Conclusion

In this dissertation, we indicated that SMS1 deficient mice showed a moderate hearing loss evaluated by sound-associated learning experiment and ABR. However, this was not shared by SMS2 deficient mice. ABR results of SMS1 KO mice showed clear hearing loss at low frequency range (4-8 kHz), while DPOAEs revealed the dysfunction of outer hair cells in the inner ear of SMS1 KO mice at mid-frequency range (8-16 kHz). The measurement of potassium concentration by double barrel microelectrode gave a similar value about 150 mM in all animals with different genotype, consistent with previous reports, whereas EP in SMS1 null mice decreased at different degrees with age. Again, SMS2 null mice had normal values both for EP and potassium concentration. We next attempted to explore the mechanism underlying hearing loss in SMS1 KO mice. Cross sections of cochlea showed remarkable atrophy of SV within which striking disorganization of marginal cell was further found by whole mount phalloidin staining. Furthermore, immunofluorescence microscopy revealed that KCNQ1 expression pattern in marginal cells was obviously altered and worsened with age. In addition, the expression level of KCNQ1 was decreased by about 60% assessed by western blotting. To explore the mechanism of frequency-dependence of hearing loss, we measured the hair cell density, KCNQ1 expression level, SV atrophy, and the pigmentation at different cochlear locations. Our observation of more macrophage invasion into SV at the apical region than the basal region may partially explain the hearing impairment at low frequency. Collectively, these data suggested that a series of defects within SV and possible impairment in hair cells may underlie EP decline and hearing impairment in SMS1 deficient mice.

References

- Anniko M & Wróblewski R (1986). Ionic environment of cochlear hair cells. *Hear Res* **22**, 279–293.
- Ashmore J (2008). Cochlear outer hair cell motility. *Physiol Rev* **88**, 173-210. Dallos P & Fakler B (2002). Prestin, a new type of motor protein. *Nat Rev Mol Cell Biol* **3**, 104-111.
- Bai Y, Wang J, Shan H, Lu Y, Zhang Y, Luo X, Yang B & Wang Z (2007). Sphingolipid metabolite ceramide causes metabolic perturbation contributing to HERG K⁺ channel dysfunction. *Cell Physiol Biochem* **20**, 429-440.
- Bosher SK & Warren RL (1978). Very low calcium content of cochlear endolymph, an extracellular fluid. *Nature* **273**, 377-378.
- Brown AM, McDowell B & Forge A (1987). Acoustic distortion products can be used to monitor the effects of chronic gentamicin treatment. *Hear Res* **42**, 14153–6.
- Chapman H, Ramström C, Korhonen L, Laine M, Wann KT, Lindholm D, Pasternack M & Törnquist K (2005). Downregulation of the HERG (KCNH2) K⁺ channel by ceramide: evidence for ubiquitin-mediated lysosomal degradation. *J Cell Sci* **118**, 5325-5334.
- Chittka L & Brockmann A (2005). Perception Space-The Final Frontier. *PLoS Biol* **3**, e137.
- Coyle B, Reardon W, Herbrick JA, Tsui LC, Gausden E, Lee J, Coffey R, Grueters A, Grossmann A, Phelps PD, Luxon L, Kendall-Taylor P, Scherer SW & Trembath RC (1998). Molecular Analysis of the Pds Gene in Pendred Syndrome (Sensorineural Hearing Loss and Goitre) (1998). *Hum Mol Genet* **7**, 1105-1112.
- Darios F, Wasser C, Shakirzyanova A, Giniatullin A, Goodman K, Munoz-Bravo JL, Raingo J, Jorgacevski J, Kreft M, Zorec R, Rosa JM, Gandia L, Gutiérrez LM, Binz T, Giniatullin R, Kavalali ET & Davletov B (2009). Sphingosine facilitates SNARE complex assembly and activates synaptic vesicle

- exocytosis. *Neuron* **62**, 683-694.
- Davis H, Fernández C & McAuliffe DR (1950). The excitatory process in the cochlea. *Proc Natl Acad Sci* **36**, 580-587.
- Ding T, Li Z, Hailemariam T, Mukherjee S, Maxfield FR, Wu M & Jiang XC (2008). SMS overexpression and knockdown: impact on cellular sphingomyelin and diacylglycerol metabolism, and cell apoptosis. *J Lipid Res* **49**, 376-385.
- Dong L, Watanabe K, Itoh M, Huan CR, Tong XP, Nakamura T, Miki M, Iwao H, Nakajima A, Sakai T, Kawanami T, Sawaki T, Masaki Y, Fukushima T, Fujita Y, Tanaka M, Yano M, Okazaki T, Umehara H (2012) CD4⁺ T-cell dysfunctions through the impaired lipid rafts ameliorate concanavalin A-induced hepatitis in sphingomyelin synthase 1-knockout mice. *Int Immunol* **24**, 327-37.
- Dror AA & Avraham KB (2010). Hearing Impairment: A panoply of genes and functions. *Neuron* **68**, 293-308.
- Dunbar GL, Lescaudron LL & Stein DG (1993). Comparison of GM1 ganglioside, AGF2, and D-amphetamine as treatments for spatial reversal and place learning deficits following lesions of the neostriatum. *Behav Brain Res* **54**, 67-79.
- Ehret G (1997). The auditory cortex. *J Comp Physiol* **181**, 547-557.
- Fay RR (1988). In: Hearing in vertebrates: a psychophysics databook. Hill-Fay associates, Winnetka, IL.
- Fettiplace R & Hackney CM (2006). The sensory and motor roles of auditory hair cells. *Nat Rev Neurosci* **7**, 19-29.
- Friedman LM, DROR AA & Avraham KB (2007). Mouse models to study inner ear development and hereditary hearing loss. *Int J Dev Biol* **51**, 609-631.
- Gow A, Davies C, Southwood C M, Frolenkov G, Chrustowski M, Ng L, Yamauchi D, Marcus D C & Kachar B (2004). Deafness in Claudin 11-null mice reveals the critical contribution of basal cell tight junctions to stria vascularis function. *J Neurosci* **24**, 7051-7062.

- Gowda S, Yeang C, Wadgaonkar S, Anjum F, Grinkina N, Cutaia M, Jiang XC & Wadgaonkar R (2011). Sphingomyelin synthase 2 (SMS2) deficiency attenuates LPS-induced lung injury. *Am J Physiol Lung Cell Mol Physiol* **300**, L430-440.
- Hannun YA & Obeid LM (2002). The Ceramide-centric universe of lipid-mediated cell regulation: stress encounters of the lipid kind. *J Biol Chem* **277**, 25847-25850.
- Helms JB & Zurzolo C (2004). Lipids as targeting signals: lipid rafts and intracellular trafficking. *Traffic* **5**, 247-254.
- Henry KR (1979). Differential changes of auditory nerve and brainstem short latency evoked potentials in the laboratory mouse. *Electroencephalogr Clin Neurophysiol* **46**, 452-459.
- Herr DR, Grillet N, Schwander M, Rivera R, Müller U & Chun J (2007). Sphingosine 1-phosphate (S1P) signaling is required for maintenance of hair cells mainly via activation of S1P2. *J Neurosci* **27**, 1474-1478.
- Hibino H, Horio Y, Inanobe A, Doi K, Ito M, Yamada M, Gotow T, Uchiyama Y, Kawamura M, Kubo T & Kurachi Y (1997). An ATP-dependent inwardly rectifying potassium channel, KAB-2 (Kir4.1), in cochlear stria vascularis of inner ear: its specific subcellular localization and correlation with the formation of endocochlear potential. *J Neurosci* **17**, 4711-4721.
- Hibino H, Nin F, Tsuzuki C & Kurachi Y (2010). How is the highly positive endocochlear potential formed? The specific architecture of the stria vascularis and the roles of the ion-transport apparatus. *Pflugers Arch* **459**, 521-533.
- Hudspeth AJ (2008). Making an Effort to Listen: Mechanical Amplification in the Ear. *Neuron* **59**, 530-545.
- Huitema K, van den Dikkenberg J, Brouwers JF & Holthuis JC (2004). Identification of a family of animal sphingomyelin synthases. *EMBO J* **23**, 33-44.
- Inokuchi J, Mizutani A, Jimbo M, Usuki S, Yamagishi K, Mochizuki H, Muramoto K, Kobayashi K,

- Kuroda Y, Iwasaki K, Ohgami Y & Fujiwara M (1997). Up-regulation of ganglioside biosynthesis, functional synapse formation, and memory retention by a synthetic ceramide analog (L-PDMP). *Biochem Biophys Res Commun* **237**, 595-600.
- Jabba SV, Oelke A, Singh R, Maganti RJ, Fleming S, Wall SM, Everett LA, Green ED & Wangemann P (2006). Macrophage invasion contributes to degeneration of stria vascularis in Pendred syndrome mouse model. *BMC Med* **4**, 37.
- Jiang H, Talaska AE, Schacht J & Sha SH (2007). Oxidative imbalance in the aging inner ear. *Neurobiol Aging* **28**, 1605-1612.
- Jung SY, Suh JH, Park HJ, Jung KM, Kim MY, Na DS & Kim DK (2000). Identification of multiple forms of membrane-associated neutral sphingomyelinase in bovine brain. *J Neurochem* **75**, 1004–1014.
- Kane KL, Longo-Guess CM, Gagnon LH, Ding D, Salvi RJ & Johnson KR (2012). Genetic background effects on age-related hearing loss associated with *Cdh23* variants in mice. *Hear Res* **283**, 80-88.
- Kemp DT (2002). Otoacoustic emissions, their origin in cochlear function, and use. *Br Med Bull* **63**, 223-241.
- Kiang NY, Rho JM, Northrop CC, Liberman MC & Ryugo DK (1982). Hair cell innervation by spiral ganglion cells in adult cats. *Science* **217**, 129-177.
- Kidani Y, Ohshima K, Sakai H, Kohno T, Baba A, Hattori M (2012) Differential localization of sphingomyelin synthase isoforms in neurons regulates sphingomyelin cluster formation. *Biochem Biophys Res Commun* **417**, 1014-1017.
- Kitajiri S, Miyamoto T, Mineharu A, Sonoda N, Furuse K, Hata M, Sasaki H, Mori Y, Kubota T, Ito J, Furuse M & Tsukita S (2004). Compartmentalization established by claudin-11-based tight junctions in stria vascularis is required for hearing through generation of endocochlear potential. *J Cell Sci* **117**, 5087-5096.
- Knipper M, Claussen C, Rüttiger L, Zimmermann U, Lüllmann-Rauch R, Eskelinen EL, Schröder J,

- Schwake M & Saftig P (2006). Deafness in LIMP2-deficient mice due to early loss of the potassium channel KCNQ1/KCNE1 in marginal cells of the stria vascularis. *J Physiol* **576**, 73-86.
- Konagaya M, Konishi T, Konagaya Y, Takayanagi T, Kita E & Muto T (1989). Partial sphingomyelinase deficiency with sea-blue histiocytosis and neurovisceral dysfunction. *Jpn J Med* **28**, 85-88.
- Konishi T & Mendelsohn M (1970). Effect of ouabain on cochlear potentials and endolymph composition in guinea pigs. *Acta Otolaryngol* **69**, 192.
- Kono M, Belyantseva IA, Skoura A, Frolenkov GI, Starost MF, Dreier JL, Lidington D, Bolz SS, Friedman TB, Hla T & Proia RL (2007). Deafness and stria vascularis defects in S1P2 receptor-null mice. *J Biol Chem* **282**, 10690-10696.
- Kujawa SG, Liberman MC (2009). Adding insult to injury: cochlear nerve degeneration after “temporary” noise-induced hearing loss. *J Neurosci* **29**, 14077–14085.
- Kusakari J, Ise I, Comegys TH, Thalmann I & Thalmann R (1978). Effect of ethacrynic acid, furosemide, and ouabain upon the endolymphatic potential and upon high energy phosphates of the stria vascularis. *Laryngoscope* **88**, 12-37.
- Lagziel A, Ahmed ZM, Schultz JM, Morell RJ, Belyantseva IA & Friedman TB (2005). Spatiotemporal pattern and isoforms of cadherin 23 in wild type and waltzer mice during inner ear hair cell development. *Dev Biol* **280**, 295-306.
- Lahiri S & Futerman AH (2007). The metabolism and function of sphingolipids and glycosphingolipids. *Cell Mol Life Sci* **64**, 2270–2284.
- Lenne PF, Wawrezynieck L, Conchonaud F, Wurtz O, Boned A, Guo XJ, Rigneault H, He HT & Marguet D (2006). Dynamic molecular confinement in the plasma membrane by microdomains and the cytoskeleton meshwork. *EMBO J* **25**, 3245-3256.
- Liberman MC (1982). The cochlear frequency map for the cat: labeling auditory-nerve fibers of known characteristic frequency. *J Acoust Soc Am* **72**, 1441–1449.

- Li Z, Zhang H, Liu J, Liang CP, Li Y, Li Y, Teitelman G, Beyer T, Bui HH, Peake DA, Zhang Y, Sanders PE, Kuo MS, Park TS, Cao G, Jiang XC (2011) Reducing plasma membrane sphingomyelin increases insulin sensitivity. *Mol Cell Biol* **31**, 4205-4218.
- Lindsay H & Norman DA (1972). Human information processing: an introduction to psychology. Academic Press, New York.
- Liu J, Huan C, Chakraborty M, Zhang H, Lu D, Kuo MS, Cao G, Jiang XC (2009). Macrophage sphingomyelin synthase 2 deficiency decreases atherosclerosis in mice. *Circ Res* **105**, 295-303.
- Luberto C, Yoo DS, Suidan HS, Bartoli GM & Hannun YA (2000). Differential effects of sphingomyelin hydrolysis and resynthesis on the activation of NF- κ B in normal and SV40-transformed human fibroblasts. *J Biol Chem* **275**, 14760–14766.
- Lukashkin AN, Richardson GP & Russell IJ (2010). Multiple roles for the tectorial membrane in the active cochlea. *Hear Res* **266**, 26–35.
- MacLennan AJ, Benner SJ, Andringa A, Chaves AH, Rosing JL, Vesey R, Karpman AM, Cronier SA, Lee N, Erway LC & Miller ML (2006). The S1P₂ sphingosine 1-phosphate receptor is essential for auditory and vestibular function. *Hear Res* **220**, 38-48.
- Marcus DC (1984). Characterization of potassium permeability of cochlear duct by perilymphatic perfusion of barium *Am J Physiol* **247**, C240-C246.
- Marcus DC, Wu T, Wangemann P & Kofuji P (2002). KCNJ10 (Kir4.1) potassium channel knockout abolishes endocochlear potential. *A J Cell Physiol* **282** , C403-C407.
- Meivar-Levy I, Sabanay H, Bershadsky AD & Futerman AH (1997). The role of sphingolipids in the maintenance of fibroblast morphology. The inhibition of protrusional activity, cell spreading, and cytokinesis induced by fumonisin B1 can be reversed by ganglioside GM3. *J Biol Chem* **272**, 1558-1564.
- Merrill AH Jr (2002). De novo sphingolipid biosynthesis: a necessary, but dangerous, pathway. *J Biol*

Chem **277**, 25843-25846.

Mihaylova V, Hantke J, Sinigerska I, Cherninkova S, Raicheva M, Bouwer S, Tincheva R, Khuyomdziev D, Bertranpetit J, Chandler D, Angelicheva D, Kremensky I, Seeman P, Tournev I & Kalaydjieva L (2007). Highly variable neural involvement in sphingomyelinase-deficient Niemann-Pick disease caused by an ancestral Gypsy mutation. *Brain* **130**, 1050-1061.

Mitsutake S, Zama K, Yokota H, Yoshida T, Tanaka M, Mitsui M, Ikawa M, Okabe M, Tanaka Y, Yamashita T, Takemoto H, Okazaki T, Watanabe K & Igarashi Y (2011). Dynamic modification of sphingomyelin in lipid microdomains controls development of obesity, fatty liver, and type 2 diabetes. *J Biol Chem* **286**, 28544-28555.

Müller M (1996). The cochlear place-frequency map of the adult and developing Mongolian gerbil. *Hearing Res* **94**, 148-156.

Müller M, von Hünenbein K, Hoidis S, Smolders JW (2005). A physiological place-frequency map of the cochlea in the CBA/J mouse. *Hear Res* **202**, 63-73.

Mustapha M, Weil D, Chardenoux S, Elias S, El-Zir E, Beckmann JS, Loiselet J & Petit C (1999). An alpha-tectorin gene defect causes a newly identified autosomal recessive form of sensorineural pre-lingual non-syndromic deafness, DFNB21. *Hum Mol Genet* **8**, 409-412.

Neyroud N, Tesson F, Denjoy I, Leibovici M, Donger C, Barhanin J, Fauré S, Gary F, Coumel P, Petit C, Schwartz K & Guicheney P (1997). A novel mutation in the potassium channel gene KVLQT1 causes the Jervell and Lange-Nielsen cardioauditory syndrome. *Nat Genet* **15**, 186-189.

Nin F, Hibino H, Doi K, Suzuki T, Hisa Y, & Kurachi Y (2008). The endocochlear potential depends on two K⁺ diffusion potentials and an electrical barrier in the stria vascularis of the inner ear. *Proc Natl Acad Sci U S A*. **105**, 1751–1756.

Nishimura M, Shirasawa H, Kaizo H & Song W-J (2007). New field with tonotopic organization in Guinea pig auditory cortex. *J Neurophysiol* **97**, 927-932.

- Noben-Trauth K, Zheng QY & Johnson KR (2003) Association of cadherin 23 with polygenic inheritance and genetic modification of sensorineural hearing loss. *Nat Genet* **35**, 21-23.
- Oghalai JS, Patel AA, Nakagawa T & Brownell WE (1998). Fluorescence-imaged microdeformation of the outer hair cell lateral wall. *J Neurosci* **18**, 48-58.
- Poleskaya O, Cunningham LL, Francis SP, Luebke AE, Zhu X, Collins D, Vasilyeva ON, Sahler J, Desmet EA, Gelbard HA, Maggirwar SB, Walton JP, Frisina RD Jr & Dewhurst S (2010). Ablation of mixed lineage kinase 3 (Mlk3) does not inhibit ototoxicity induced by acoustic trauma or aminoglycoside exposure. *Hear Res* **270**, 21-27.
- Probst FJ, Camper SA (1999). The role of mouse mutants in the identification of human hereditary hearing loss genes. *Hear Res* **130**, 1-6.
- Ramu Y, Xu Y & Lu Z (2006). Enzymatic activation of voltage-gated potassium channels. *Nature* **442**, 696-699.
- Riazuddin S, Ahmed ZM, Fanning AS, Lagziel A, Kitajiri S, Ramzan K, Khan SN, Chattaraj P, Friedman PL, Anderson JM, Belyantseva IA, Forge A, Riazuddin S & Friedman TB (2006). Tricellulin is a tight-junction protein necessary for hearing. *Am J Hum. Genet* **79**, 1040-1051.
- Riboni L, Viani P, Bassi, R, Giussani, P & Tettamanti, G (2001). Basic fibroblast growth factor-induced proliferation of primary astrocytes: evidence for the involvement of sphingomyelin biosynthesis. *J. Biol. Chem* **276**, 12797-12804.
- Rickheit G, Maier H, Strenzke N, Andreescu CE, De Zeeuw CI, Muenscher A, Zdebik AA & Jentsch TJ (2008). Endocochlear potential depends on Cl⁻ channels: mechanism underlying deafness in Bartter syndrome IV. *EMBO J* **27**, 2907–2917.
- Rzadzinska AK, Derr A, Kachar B, Noben-Trauth K (2005) Sustained cadherin 23 expression in young and adult cochlea of normal and hearing-impaired mice. *Hear Res* **208**, 114-121.
- Sakagami M, Fukazawa K, Matsunaga T, Fujita H, Mori N, Takumi T, Ohkubo H & Nakanishi S (1991).

- Cellular localization of rat Isk protein in the stria vascularis by immunohistochemical observation. *Hear Res* **56**, 168–172.
- Schulte BA & Schmiedt RA (1992). Lateral wall Na, K-ATPase and endocochlear potentials decline with age in quiet-reared gerbils. *Hear Res* **61**, 35–46.
- Simons K & Toomre D (2000). Lipid rafts and signal transduction. *Nat Rev Mol Cell Biol* **1**, 31-39.
- Singh R & Wangemann P (2008). Free radical stress-mediated loss of Kcnj10 protein expression in stria vascularis contributes to deafness in Pendred syndrome mouse model. *Am J Physiol Renal Physiol* **294**, F139-148.
- Spiegel S & Milstien S (2002). Sphingosine 1-phosphate, a key cell signaling molecule. *J Biol Chem* **277**, 25851-25854.
- Staecker H, Zheng QY & Van De Water TR (2001). Oxidative stress in aging in the C57B16/J mouse cochlea. *Acta Otolaryngol* **121**, 666-672.
- Subathra M, Qureshi A & Luberto C (2011). Sphingomyelin synthases regulate protein trafficking and secretion. *PLoS ONE* **6**, e23644.
- Tafesse FG, Huitema K, Hermansson M, van der Poel S, van den Dikkenberg J, Uphoff A, Somerharju P, & Holthuis JC (2007). Both Sphingomyelin synthases SMS1 and SMS2 are required for sphingomyelin homeostasis and growth in human HeLa cells. *J Biol Chem* **282**, 17537-17547.
- Tafesse FG, Ternes P & Holthuis JC (2006). The multigenic sphingomyelin synthase family. *J Biol Chem* **281**, 29421-29425.
- Takeuchi S, Ando M & Kakigi A (2000). Mechanism generating endocochlear potential: role played by intermediate cells in stria vascularis. *Biophys J* **79**, 2572-2582.
- Tasaki I & Spyropoulos CS (1959). Stria vascularis as source of endocochlear potential. *J Neurophysiol* **22**, 149-155.
- Teubner B, Vincent Michel, Pesch J, Lautermann J, Cohen-Salmon M, Söhl G, Jahnke K, Winterhager

- E, Herberhold C, Hardelin JP, Petit C & Willecke K (2003). Connexin30 (Gjb6)-deficiency causes severe hearing impairment and lack of endocochlear potential. *Hum Mol Genet* **12**, 13-21.
- Tsukamoto K, Suzuki H, Harada D, Namba A, Abe S & Usami S (2003). Distribution and frequencies of PDS (SLC26A4) mutations in Pendred syndrome and nonsyndromic hearing loss associated with enlarged vestibular aqueduct: a unique spectrum of mutations in Japanese. *Eur J Hum Genet* **11**, 916-922.
- Uyguner O, Emiroglu M, Uzumcu A, Hafiz G, Ghanbari A, Baserer N, Yuksel-Apak M & Wollnik B (2003). Frequencies of gap- and tight-junction mutations in Turkish families with autosomal-recessive non-syndromic hearing loss. *Clin Genet* **64**, 65-9.
- Van Meer G & Hoetzel S (2010). Sphingolipid topology and the dynamic organization and function of membrane proteins. *FEBS Letters*, **584**, 1800-1805.
- Verhoeven K, Van Laer L, Kirschhofer K, Legan PK, Hughes DC, Schatteman I, Verstreken M, Van Hauwe P, Coucke P, Chen A, Smith RJH, Somers T, Offeciers FE, Van de Heyning P, Richardson GP, Wachtler F, Kimberling WJ, Willems PJ, Govaerts PJ & Van Camp, G (1998). Mutations in the human α -tectorin gene cause autosomal dominant non-syndromic hearing impairment *Nat. Genet* **19**, 60-62.
- Wallace MN, Rutkowski RG, Palmer AR (2000). Identification and localization of auditory areas in guinea pig cortex. *Exp Brain Res* **132**, 445-456.
- Walsh T, Walsh V, Vreugde S, Hertzano R, Shahin H, Haika S, Lee MK, Kanaan M, King MC & Avraham KB. (2002). From flies' eyes to our ears: mutations in a human class III myosin cause progressive nonsyndromic hearing loss DFNB30. *Proc Natl Acad Sci* **99**, 7518-7523.
- Wangemann P (2002). K⁺ cycling and the endocochlear potential. *Hear Res* **165**, 1-9. Xu Y, Ramu Y & Lu Z (2008). Removal of phospho-head groups of membrane lipids immobilizes voltage sensors of K⁺ channels. *Nature* **451**, 826-829.
- Wangemann P, Itza EM, Albrecht B, Wu T, Jabbaal SV, Maganti RJ, Lee JH, Everett LA, Wall SM,

- Royaux IE, Green ED & Marcus DC (2004). Loss of KCNJ10 protein expression abolishes endocochlear potential and causes deafness in Pendred syndrome mouse model. *BMC Med* **2**, 30.
- Wilcox ER, Burton QL, Naz S, Riazuddin S, Smith TN, Ploplis B, Belyantseva I, Ben-Yosef T, Liburd NA, Morell RJ, Kachar B, Wu DK, Griffith AJ, Riazuddin S & Friedman TB (2001). Mutations in the gene encoding tight junction claudin-14 cause autosomal recessive deafness DFNB29. *Cell* **104**, 165–172.
- Xu Y, Ramu Y & Lu Z (2008). Removal of phospho-head groups of membrane lipids immobilizes voltage sensors of K⁺ channels. *Nature* **451**, 826-829.
- Yamagata K, Senokuchi T, Lu M, Takemoto M, Fazlul Karim M, Go C, Sato Y, Hatta M, Yoshizawa T, Araki E, Miyazaki J & Song WJ (2011). Voltage-gated K⁺ channel KCNQ1 regulates insulin secretion in MIN6 β -cell line. *Biochem Biophys Res Commun* **407**, 620-625.
- Yamaoka S, Miyaji M, Kitano T, Umehara H & Okazaki T (2004). Expression cloning of a human cDNA restoring sphingomyelin synthesis and cell growth in sphingomyelin synthase-defective lymphoid cells. *J Biol Chem* **279**, 18688-18693.
- Yano M, Watanabe K, Yamamoto T, Ikeda K, Senokuchi T, Lu M, Kadomatsu T, Tsukano H, Ikawa M, Okabe M, Yamaoka S, Okazaki T, Umehara H, Gotoh T, Song WJ, Node K, Taguchi R, Yamagata K & Oike Y (2011). Mitochondrial dysfunction and increased reactive oxygen species impair insulin secretion in sphingomyelin synthase 1-null mice. *J Biol Chem* **286**, 3992-4002.
- Yang Z, Jean-Baptiste G, Khoury C & Greenwood MT (2005). The mouse sphingomyelin synthase 1 (SMS1) gene is alternatively spliced to yield multiple transcripts and proteins. *Gene* **363**, 123-132.
- Yorgason JG, Fayad JN & Kalinec F (2006). Understanding drug ototoxicity: molecular insights for prevention and clinical management. *Expert Opin Drug Saf* **5**, 383-399.
- Yoshikawa M, Go S, Takasaki K, Kakazu Y, Ohashi M, Nagafuku M, Kabayama K, Sekimoto J, Suzuki S, Takaiwa K, Kimitsuki T, Matsumoto N, Komune S, Kamei D, Saito M, Fujiwara M, Iwasaki K &

- Inokuchi J (2009). Mice lacking ganglioside GM3 synthase exhibit complete hearing loss due to selective degeneration of the organ of Corti. *Proc Natl Acad Sci* **106**, 9483-9488.
- Zdebik AA, Wangemann P, Jentsch TJ (2009). Potassium ion movement in the inner ear: insights from genetic disease and mouse models. *Physiology* **24**,307-316.
- Zeidan YH, Jenkins RW & Hannun YA (2008). Remodeling of cellular cytoskeleton by the acid sphingomyelinase/ceramide pathway. *J Cell Biol* **181**, 335-350.
- Zhang Y, Dong J, Zhu X, Wang W & Yang Q (2011). The effect of sphingomyelin synthase 2 (SMS2) deficiency on the expression of drug transporters in mouse brain. *Biochem Pharmacol* **82**, 287-294.